STUDIES ON THE PULSED UV LASERS EXCITED BY LONGITUDINAL DISCHARGE WITH AUTOMATIC PREIONIZATION

Hideo FURUHASHI and Toshio GOTO

Department of electronics

(Received October 30, 1990)

Abstract

Pulsed UV lasers (N_2 and XeCl excimer lasers) excited by longitudinal discharge with automatic preionization have been studied. By using spark UV preionization and a charge transfer excitation circuit, the laser performance has been considerably improved.

When the laser system was operated as a XeCl excimer laser, laser pulses of about 200 μJ output energy, 15 ns width (FWHM) and 1 mrad beam divergence (full angle) were obtained in the compact laser system of 26 cm discharge length at the gas mixture of 1.3 atm (He:Xe:HCl = 1.3 atm:6.0 torr:2.4 torr) and driving voltage of 40 kV.

When the laser system was operated as a low pressure N_2 laser (337 nm), laser pulses of about 65 kW peak power and 5 ns width (FMHM) were obtained at the N_2 gas pressure of 60 torr and driving voltage of 40 kV.

By using a rectangular cross-section discharge tube instead of a circular cross-section discharge tube, the performance of an N_2 laser has been improved considerably, and laser pulses of about 160 kW peak power, 1.28 mJ output energy and 8 ns pulse width (FWHM) were obtained.

The possibilities of the high repetition rate operation have been investigated for N_2 laser and XeCl excimer laser. For N_2 laser, maximum average output power above 100 mW was obtained at the repetition rate of 130 pps.

Contents

1. Introduction

In three decades after the first observation of the laser action in ruby in 1960, lasers left the field of research laboratories and penetrated expanding new markets in commercial and industrial products and systems. Laser action was observed in the wide wavelength region. Especially, many efforts have been made for short wavelength lasers. Although soft X-ray laser action was reported in laser-produced plasma, practical short wavelength lasers, such as discharge pumped excimer and N_2 lasers, operate at UV region. Such lasers are applicable to material processing, medical treatment, spectroscopy, and studies of physical properties.[1]

Although the excitation mechanisms of excimer and N_2 lasers are not the same, the excitation requirements are similar to each other; high power deposition, fast excitation of several ns and uniform discharge. Therefore these lasers can be operated using almost the same laser systems for different gas mixtures. The laser action of these laser systems is accomplished in a variety of ways; electron beam, electron beam sustained discharge, self-sustained discharge, etc.[2-12] Such lasers using electron beam excitation are favorable for obtaining high laser

power, but they are not suitable for commercial applications, because they are complex and expensive and can't operate at high repetition rate. On the other hand, lasers using discharge excitation are simple and can operate at higher repetition rate than those using electron beam excitation.

The early discharge pumped rare gas halide excimer lasers were operated with transversal discharge excitation in which the laser beam axis is perpendicular to the discharge electric field.[11-16] Many investigations were made about them. On the other hand, investigations on longitudinal discharge excitation, in which the laser beam axis is in parallel with the discharge electric field, are very few. In the seventies, only one investigation on the longitudinal discharge excimer laser was reported for XeF excimer.[17] In the eighties, some investigations on this type of laser were reported for XeF, XeCl and KrF excimer.[18-22] There are also two types of the excitation methods for N_2 lasers excited by discharge; longitudinal discharge[23-25] and transversal discharge.[3] Although the longitudinal discharge lasers are lower at the powers than the transversal discharge lasers, the formers are simpler and more compact in construction.

For obtaining high output power, a fast and uniform arc-free discharge of large current and high voltage is demanded. In the case of the transversal discharge UV lasers, it was realized by using spark UV photo-preionization,[14] corona preionization,[26] and X-ray preionization,[27] and remarkable increase in output powers could be obtained. On the other hand, for longitudinal discharge UV lasers, there was no attempt of effective preionization.

The purpose of this study is to design and construct a simple and compact UV laser with high reliability, and solidify the foundation of the laser system. To achieve this object, longitudinal discharge excitation has been investigated and some new designs of the laser system have been proposed in this study; (1) longitudinal discharge UV laser with automatic UV spark preionization, (2) longitudinal discharge UV laser using combined excitation circuit of charge transfer circuit with LC-inversion circuit, (3) longitudinal discharge UV laser with rectangular cross-section. By using these new laser systems, studies of the preionization, the excitation circuit and the laser head structure have been done. Furthermore, operation at high repetition rate using thyratron has been investigated.

2.   Longitudinal Discharge XeCl Excimer Laser with Automatic Preionization

Although many kinds of preionization techniques are normally used for transversal discharge excimer lasers[14,26,27] to obtain uniform and high current discharge, strong preionization such as spark UV preionization has never been used for longitudinal discharge rare-gas halide excimer lasers.

In this chapter, a new design of the longitudinal discharge excitation system is proposed; longitudinal discharge laser with automatic spark UV preionization. It is the first time that spark UV preionization is used for a longitudinal discharge laser. As the first step of the study, it is operated as a XeCl excimer laser, and the characteristics of the laser performance have been investigated.

2.1.   Experimental

Fig. 2.1 shows the schematic diagram of the basic excitation scheme of the longitudinal discharge laser with automatic spark UV preionization. When the spark gap switch is closed, rapidly rising high voltage appears between the electrode pins (P_0-P_1, Q_0-Q_1) through the capacitor C_0. Then these small gaps reach their breakdown voltage and are bridged by sparks.

The UV radiation generated by these sparks preionizes the gas in the capillary. At the same time, the capacitor C_0 is charged up by the current from the capacitor C_1. When the spark UV preionization proceeds and the capacitor C_0 is charged up to the breakdown voltage between the electrode pins P_0 and Q_0, the main longitudinal discharge occurs along the tube axis, and the capacitor C_0 discharges. By using spark UV preionization, we can obtain many initial electrons in the capillary, resulting in discharge of more uniform and higher electron density, and higher energy is loaded to the gas in the capillary in a very short time.
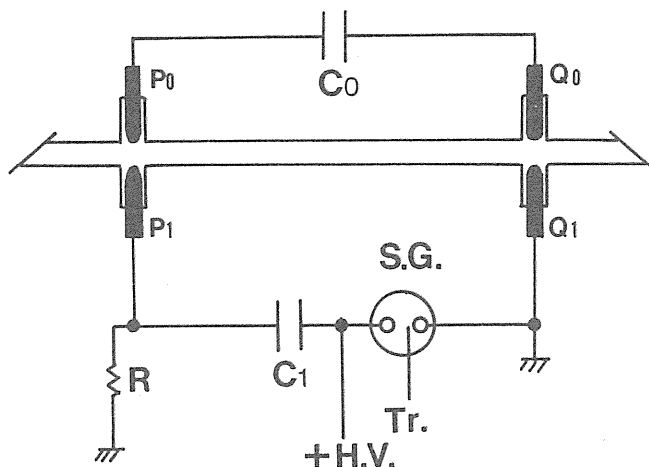
Fig. 2.1. Schematic diagram of the basic excitation scheme of the longitudinal discharge laser with automatic spark preionization. S.G.: spark gap switch, Tr.: trigger.

Fig. 2.2 shows the schematic diagram of the laser system used in this experiment. The laser tube consists of four-segmented longitudinal discharge tube. Four Teflon pipes are connected to each other with five Teflon pipe fittings. One segment of the tube has a length of 65 mm and an inner diameter of 4 mm, thus the discharge channel has a total length of 260 mm and a volume of about 3.3 cm^3. Five pairs of electrodes are used, and each pair consists of two stainless pins separated by a small gap of 4 mm for sprak UV preionization. The output Brewster windows are made of quartz.

The capacitors C_0 and C_1 are commercially available doorknob capacitors. A two-stage Marx bank generator is used for providing high voltage pulses. By triggering the spark gap S.G.$_1$ and closing it, the spark gap S.G.$_2$ closes automatically, and double voltage of the charging voltage is supplied to the laser tube. The two capacitors C_1 are charged with a high voltage power supply. Since the capacitance of C_1 is 6800 pF, the storage capacitance per segment is 850 pF. Each of the peaking capacitors C_0 has a capacitance of 560 pF. The peaking capacitors are mounted on the laser tube as near as possible and are directly connected to the two electrode pins P_0 and Q_0 by copper plates for decreasing the inductance of the excitation circuit.

The optical resonator is composed of two external dielectric mirrors separated by 600 mm, one of which is a total reflector (T.R.) and the other is a 95% reflecting partial reflector (P.R.) with a 5 m radius of curvature.

In this experiment, the laser pulse shapes were observed using a biplanar phototube R1193U-2 (Hamamatsu Photonics K.K.), and the laser pulse energy measurements were carried out by using a volume absorbing disk calorimeter Scientech 38-0105. The measurements of the spontaneous emission pulses were made with a photomultiplier 1P21 (Hamamatsu Photonics K.K.) and a monochromator. The discharge-current pulses and the voltage pulses were observed using an one-turn Rogowski coil and a $CuSO_4$ voltage divider, respectively.
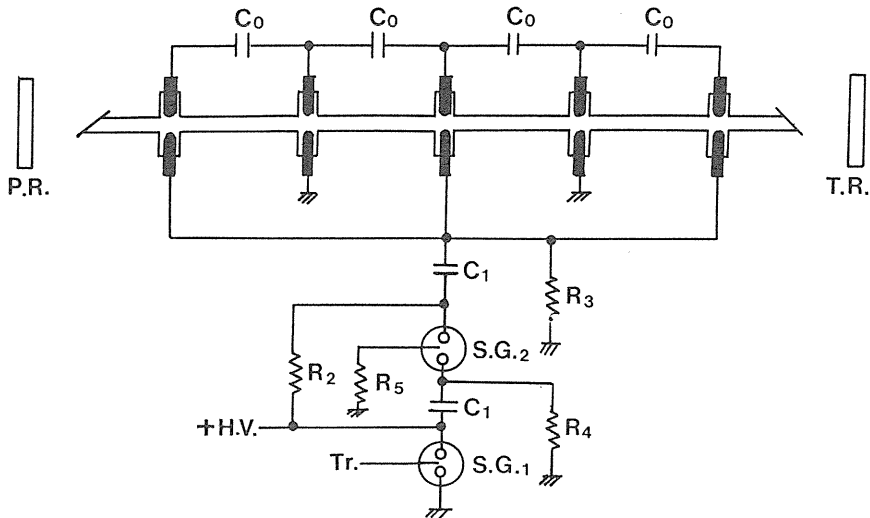

Fig. 2.2. Schematic diagram of the laser system used in this experiment. S.G.: spark gap, Tr. trigger, T.R.: total reflector, P.R.: partial reflector. $C_0 = 560\,pF$, $C_1 = 6800\,pF$, $R_2 = 2\,M\Omega$, $R_3 = 20$ $k\Omega$, $R_4 = 3\,k\Omega$, $R_5 = 30\,k\Omega$.

2.2. Results and Discussion

2.2.1. Oscillation of the Longitudinal Discharge XeCl Excimer Laser with Spark UV Pre-ionization

Fig. 2.3 shows the time behavior of the waveforms; discharge voltage, current, spontaneous emission and laser pulse (308 nm) at a mixture of He:Xe:HCl = 99.3:0.5:0.2 and the total gas pressure of 1.5 atm. The driving voltage (twice the charging voltage) is 40 kV. When the spark gap switches are closed, the voltage V_1 increases. About 40 ns after the close of the spark gaps, the spark UV preionization starts (I_0 and I_1) and the voltage V_0 increases. About 40 ns after the start of the preionization, the longitudinal discharge occurs (I_2) and the laser pulse is obtained soon afterwards. Most of the longitudinal discharge current flows from the peaking capacitor C_0. This is because the inductance of the excitation circuit composed of the peaking capacitor is smaller than that composed of the capacitor C_1 and spark gap switches. The full width at half maximum (FWHM) of the laser pulse is about 15 ns and the spontaneous emission pulse is longer than that.

About 15 ns time lag of the laser pulse is observed behind the longitudinal discharge current I_2. This is provably due to the formation process of XeCl* excimer molecules. It is
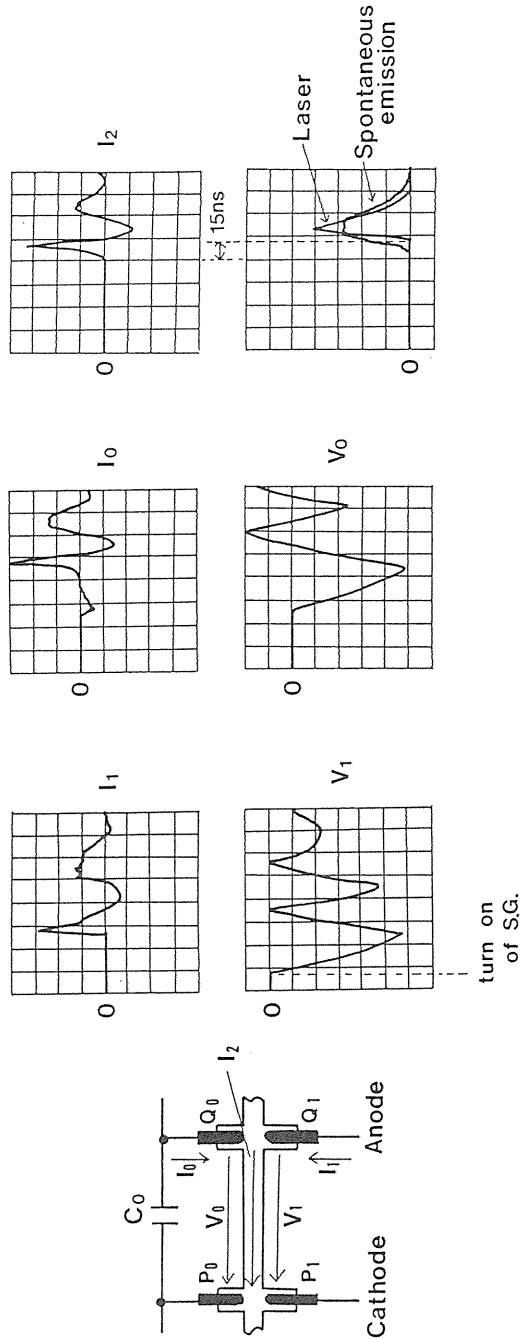
Fig. 2.3. Time behaviors of the waveforms. Discharge voltage, current, spontaneous emission, and laser pulse (308 nm). He:Xe:HCl = 99.3:0.5:0.2, total pressure 1.5 atm, driving voltage 40 kV. Horizontal axis: 20 ns/div. Vertical axis: arbitrary units.

believed that, during the initial stage of the discharge, the main channel of the formation of the XeCl* excimer molecules is the harpoon reaction.[28,29)]

$$Xe^* + HCl\,(\nu) \rightarrow XeCl^* + H \qquad\qquad (2.1)$$

In this stage the time dependences of the small-signal gain and the spontaneous emission of XeCl* coincide with that of the discharge current waveform. However, the main formation process of XeCl* excimer molecules is three-body ion-ion recombination.[28-30)]

$$Xe^* + Cl^- + He \rightarrow XeCl^* + He \qquad\qquad (2.2)$$

The main mechanism of the formation of the Cl$^-$ ions in the discharge is the dissociative trapping of electrons.[28-30)]

$$HCl\,(\nu) + e \rightarrow Cl^- + H \qquad\qquad (2.3)$$

The rate of this reaction depends strongly on the electron energy and on the degree of vibrational excitation of HCl. In the initial stage of the discharge, the average electron energy is high, but the concentration of the vibrationally excited HCl (ν) molecules is low, thus the process of the formation of Cl$^-$ is slow. Therefore, time lag of laser is observed behind the longitudinal discharge current. These time behaviors of the XeCl* excimer molecules, Cl$^-$ ions and discharge current were reported by V.E. Peet and A.B. Treshchalov for transversal discharge XeCl laser by the method of absorption probing with tunable dye laser pulses.[28)] (Fig. 2.4)
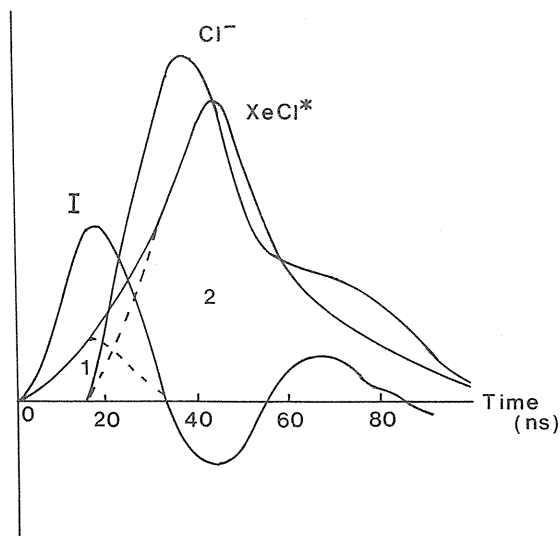

Fig. 2.4. Time behaviors of the XeCl* excimer molecules, Cl$^-$ ions and discharge current, investigated by V.E. Peet and A.B. Treshchalov (ref. 28). Region 1: harpoon reaction, region 2: ion-ion recombination.

2.2.2. *Effects of the Preionization and Charge Transfer Circuit on the Laser Performance*

Fig. 2.5 shows three types of excitation circuits used for investigating the effects of spark UV preionization and charge transfer circuit on the laser performance. Here the two-stage Marx bank generator is not shown. The first type of laser has been operated without the spark UV preionization or peaking capacitor C_0 (type 1); the second has been operated without the spark UV preionization but by connecting the peaking capacitor C_0 between the electrode pins P_1 and Q_1 (type 2); the third has been operated with the spark UV preionization and by connecting the peaking capacitor C_0 between the electrode pins P_0 and Q_0 (type 3).
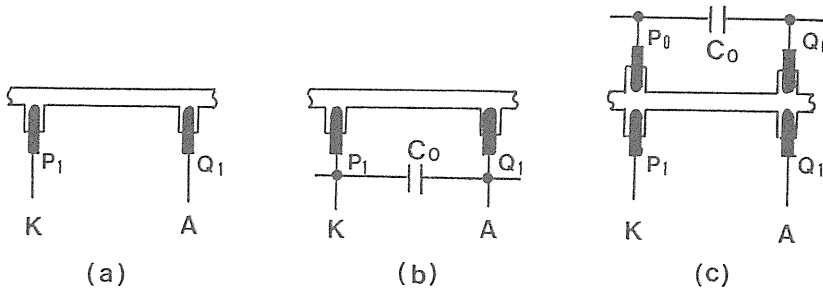
Fig. 2.5. Experimental excitation circuit. (a) type 1: without charge transfer circuit and spark preionization, (b) type 2: with charge transfer circuit but without spark preionization, (c) type 3: with charge transfer circuit and spark preionization.

Fig. 2.6 shows the dependence of the laser peak power on the total gas pressure for the type 2 and type 3 lasers at a gas mixture of Ne:Xe:HCl = 95.6:4.1:0.3. The driving voltage is

Fig. 2.6. Dependence of the laser peak power on the total gas pressure. Ne:Xe:HCl = 95.6:4.1:0.3, driving voltage 40 kV. Type 2 laser (○), type 3 laser (●).

40 kV. When the type 1 laser was used, no laser oscillation was obtained. This result shows that the charge transfer circuit is effective for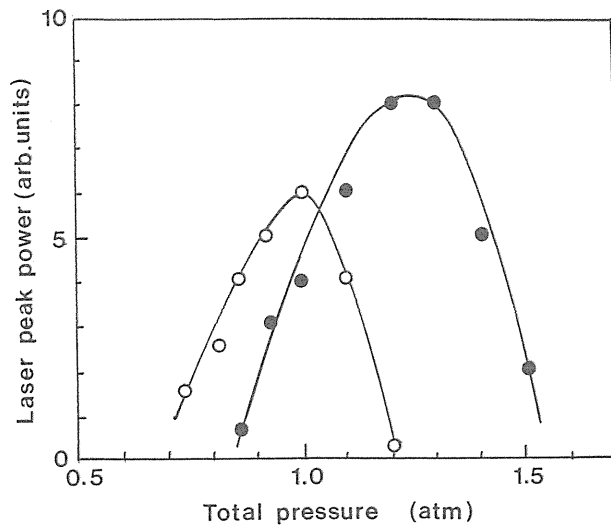 increasing the laser power. This is because, the inductance of the Marx bank pulse generator is not very low, but the inductance of the excitation circuit is decreased by using the charge transfer circuit. As a result, large-current and high-voltage discharge is obtained. Furthermore, the laser peak power of the type 3 laser is higher than that of the type 2 laser. This result shows that the spark UV preionization is also effective for increasing the laser peak power. This is because an uniform and large-current discharge is obtained by using the preionization. The laser peak power has maximum for the type 2 and type 3 lasers. The optimum total gas pressure for the type 3 laser is higher than that of the type 2 laser. At a low gas pressure, the laser peak power of the type 3 laser is lower than that of the type 2 laser. This is probably because the breakdown voltage is decreased by using the spark UV preionization.

Furthermore, by using the spark UV preionization, the shot-to-shot reproducibilities of the laser power and the laser pulse shape were improved.

In conclusion, the good effects of the charge transfer circuit and the spark UV preionization on the laser performance have been confirmed.

2.2.3. Optimization of the Gas Mixtures

In the case of a XeCl excimer laser excited by discharge, generally a mixture of Xe, HCl and a buffer gas is used. The concentrations of these gases have large influences on the laser performance. The role of these gases are shown below.

(a) HCl

As a halogen donor of XeCl excimer laser, some gases such as Cl_2,[7] BCl_3,[11] CCl_4,[31] or HCl[15,32] were used. HCl is generally used as a halogen donor because of the low photoabsorption of 308 nm.

HCl plays important roles on the laser performance as shown below.[33]

I. Formation of XeCl*

$$Xe^+ + Cl^- + M \rightarrow XeCl^* + M \qquad (2.4)$$

$$MXe + Cl^- \rightarrow XeCl^* + M + e \qquad (2.5)$$

$$Xe^* + HCl\,(v) \rightarrow XeCl^* + H \qquad (2.6)$$

$$Xe_2 + Cl^- \rightarrow XeCl^* + Xe + e \qquad (2.7)$$

(M: buffer gas)

II. Quenching of XeCl*

$$XeCl^* + HCl \rightarrow Xe + Cl + HCl \qquad (2.8)$$

$$XeCl^* + HCl\,(v) \rightarrow Xe + Cl + HCl \qquad (2.9)$$

III. Photoabsorption of 308 nm

$$Cl^- + h\nu \rightarrow Cl + e \qquad (2.10)$$
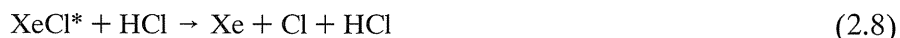
IV.   Dissociative attachment of electron

$$HCl\,(v) + e \rightarrow H + Cl^{-} \tag{2.11}$$

As a result of the dissociative attachment of electron, an increase in the concentration of HCl causes the decrease in the electron density, and the discharge impedance increases. At the same time, HCl decreases the electron energy owing to the large vibrational-excitation cross sections in the order of 10^{-15} cm^2.[34] Furthermore it is believed this dissociative attachment causes inhomogeneous discharge.[33,35,36] In an XeCl laser gas mixture, the chlorine atoms recombine with hydrogen atoms to form HCl on a time scale which is slow compared to the duration of the laser output pulse. The concentration of the halogen donor is, therefore, progressively reduced throughout the duration of the laser pulse. If an excess of electrons occurs at some point in space, the halogen donor at the point decreases faster than the ambient. Since dissociative attachment of electron with halogen donor is a dominant electron loss process, this will reduce the local electron loss rate, and a greater excess of electrons occurs. As a result, some low impedance discharge channel is produced locally, and filamentation discharge occurs.

(b)   Xe
    Xe plays important roles on the laser performance as shown below.[33]
I.   Formation of XeCl*

$$Xe^{+} + Cl^{-} + M \rightarrow XeCl^{*} + M \tag{2.4}$$

$$MXe + Cl^{-} \rightarrow XeCl^{*} + M + e \tag{2.5}$$

$$Xe^{*} + HCl\,(v) \rightarrow XeCl^{*} + H \tag{2.6}$$

$$Xe_2 + Cl^{-} \rightarrow XeCl^{*} + Xe + e \tag{2.7}$$

(M: buffer gas)

II.   Quenching of XeCl*

$$XeCl^{*} + Xe \rightarrow 2Xe + Cl \tag{2.12}$$

III.   Photoabsorption of 308 nm

$$Xe_2^{+} + h\nu \rightarrow Xe^{+} + Xe \tag{2.13}$$

$$Xe^{*} + h\nu \rightarrow Xe^{+} + e \tag{2.14}$$

IV.   Formation of electron

$$Xe^{*} + e \rightarrow Xe^{+} + 2e \tag{2.15}$$

$$Xe + e \rightarrow Xe^{+} + 2e \tag{2.16}$$

Because these ionization processes of Xe are dominant electron formation processes, large concentration of Xe has a tendency to cause an inhomogeneous discharge.[33]

(c) Buffer gas

A lighter rare gas is generally used as a bufffer gas. The roles of the buffer gas on the laser performance are shown below.[33]

I. Formation of XeCl*

$$Xe^+ + Cl^- + M \rightarrow XeCl^* + M \qquad (2.4)$$

$$MXe + Cl^- \rightarrow XeCl^* + M + e \qquad (2.5)$$

II. Quenching of XeCl*

$$XeCl^* + M \rightarrow Xe + Cl + M \qquad (2.17)$$

Furthermore buffer gas determines the electron energy distribution dominantly.

He, Ne, or Ar is generally used as a buffer gas of XeCl excimer laser because of the good discharge stability. These gases have characteristics as shown in table 2.1. From the view point of the discharge stability, He gas is the best, because the ionization energy is high. However, from the view point of the electron density, Ne gas is the best. This is because the momentum transfer cross section of Ne is smaller than that of He or Ar, and the electrons of high energy increase. The dominant electron formation processes are the direct and two step ionizations of Xe, and the energies required for reactions $Xe \rightarrow Xe^+ + e$, $Xe + e \rightarrow Xe^* + e$, and $Xe^* + e \rightarrow Xe^+ + 2e$ are 12.1, 8.3 and 3.8 eV, respectively. Because of the large density of high-energy electrons in Ne/Xe/HCl and Ar/Xe/HCl gas mixtures, the ionization rate in them is larger than that of He/Xe/HCl gas mixture. Thus the electron densities in Ne/Xe/HCl and Ar/Xe/HCl gas mixtures are larger than that in He/Xe/HCl gas mixture. On the other hand, a rate for an electron attachment to HCl molecule, which is a dominant electron loss process, is higher for He/Xe/HCl gas mixture than for Ne/Xe/HCl gas mixture at the same E/P value.[30] Therefore, the operating E/P value for He/Xe/HCl gas mixture becomes higher than that for Ne/Xe/HCl gas mixture so that the electron ionization may be balanced with the electron attachment. Thus the discharge impedance of the former is higher than that of the latter.[30,37]

Table 2.1. Characteristics of buffer gases.

	He	Ne	Ar
Ionization energy	24.6 eV	21.6 eV	15.8 eV
Metastable energy	19.8 eV	16.5 eV	11.5 eV
Discharge stability	good	→	poor
Contribution to excimer formation	poor	←	good
Distribution of electron energy	poor ←	good →	poor
Quenching of excimer	small	→	large
Discharge impedance	high →	low ←	high

On the other hand, the dominant quenching of XeCl* is the quenching by electron, and the quenching rate is large $(1.2 \times 10^{-7}\,\mathrm{cm^3 \cdot s^{-1}})$.[33] The quenching of XeCl* in He buffer gas is smaller than that in Ne buffer gas because of the smaller electron density. The reaction rate of the three-body ion-ion recombination $\mathrm{Xe^+ + Cl^- + M \rightarrow XeCl^* + M}$, which is a predominant XeCl* formation channel, is $1.3 \times 10^{-7}\,\mathrm{cm^3 \cdot s^{-1}}$ for He gas and $1.4 \times 10^{-6}\,\mathrm{cm^3 \cdot s^{-1}}$ for Ne gas.[33] Thus Ne gas is better than He gas for the formation of XeCl*.

Laser performance strongly depends on the concentrations of these gases. Therefore the gas mixtures are optimized for He/Xe/HCl and Ne/Xe/HCl gas mixtures. Laser oscillation was not obtained for Ar/Xe/HCl gas mixtures.

Figs. 2.7 show the dependences of the laser peak power on the several Xe and HCl partial pressures for Ne/Xe/HCl and He/Xe/HCl gas mixtures. In Figs. 2.7 (a) and (a′) HCl partial pressure is kept constant at 2.4 torr, and Xe partial pressure is changed. In Figs. 2.7 (b) and (b′), Xe partial pressures are kept constant at 12 torr and 6.0 torr, respectively, and HCl partial pressure is changed. The total gas pressure is varied from 1.0 to 1.5 atm. The optimum partial pressures of Xe and HCl for Ne/Xe/HCl gas mixture are about 12 torr and 2.4 torr, respectively. On the other hand those for He/Xe/HCl gas mixture are about 6.0 and 2.4 torr, respectively.

There are optimum partial pressures of Xe and HCl. This is because, when the partial pressure of Xe is increased, the formation rate of XeCl* by the reactions (2.4)–(2.7) increases. Furthermore, the electron density is increased by the reactions (2.15) and (2.16).
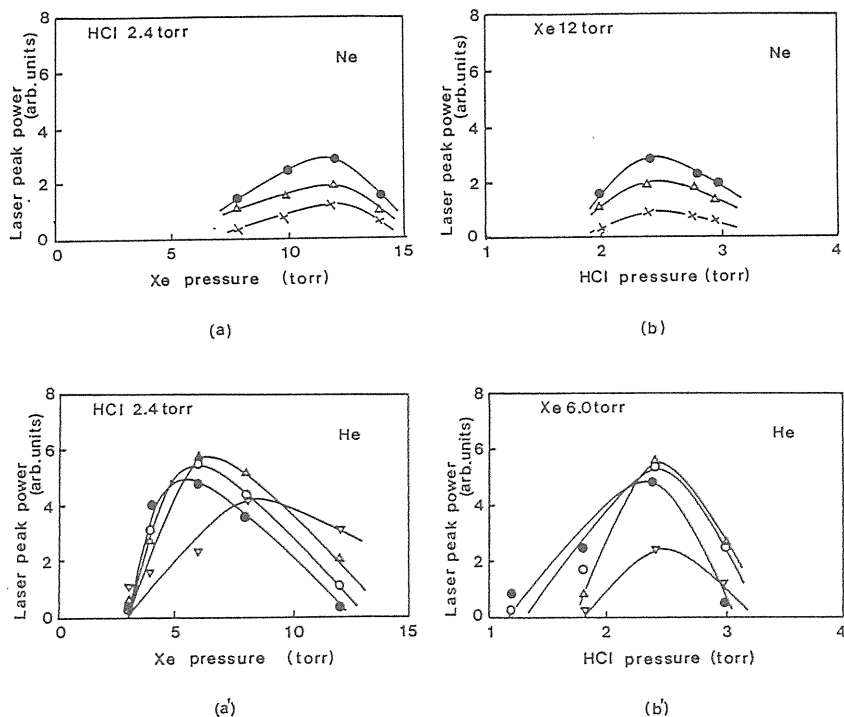

Fig. 2.7. Dependences of the laser peak powers on the Xe and HCl partial pressures for Ne/Xe/HCl and He/Xe/HCl mixtures. Driving voltage 40 kV. Total gas pressure 1.0 atm (×), 1.2 atm (▽), 1.3 atm (△), 1.4 atm (○), 1.5 atm (●).

However, the discharge impedance decreases at higher Xe partial pressures, and the increase in low energy electrons causes an increase in quenching of XeCl* by the reaction XeCl* + e → Xe + Cl + e, which is a dominant loss process of XeCl*.[30] Next, when partial pressure of HCl is increased, the formation rate of XeCl* by the reactions (2.4)–(2.7) also increases. However, the electron density is decreased by the dissociative attachment (2.11), which is a dominant loss process of electrons. Furthermore the photoabsorption of 308 nm laser radiation by Cl⁻ + hν → Cl + e increases, and at high HCl partial pressure, the quenching of XeCl* by the reactions XeCl* + HCl → Xe + Cl + HCl and XeCl* + HCl(ν) → Xe + Cl + HCl increases. Thus there are optimum partial pressures of Xe and HCl.

Fig. 2.8 shows the comparison of the laser performances using He/Xe/HCl and Ne/Xe/HCl gas mixtures. It shows the dependence of the laser peak power on the buffer gas pressure in the optimum gas mixtures. The driving voltage is 40 kV. The laser peak power using He/Xe/HCl gas mixture is higher than that using Ne/Xe/HCl gas mixture. In a transversal discharge XeCl laser, better laser performance is generally obtained by using Ne/Xe/HCl gas mixture owing to the high reaction rate of the three-body ion-ion recombination Xe⁺ + Cl⁻ + Ne → XeCl* + Ne. The result obtained in this experiment is probably due to the low energy deposition for Ne/Xe/HCl gas mixture. In the case of a longitudinal discharge excimer
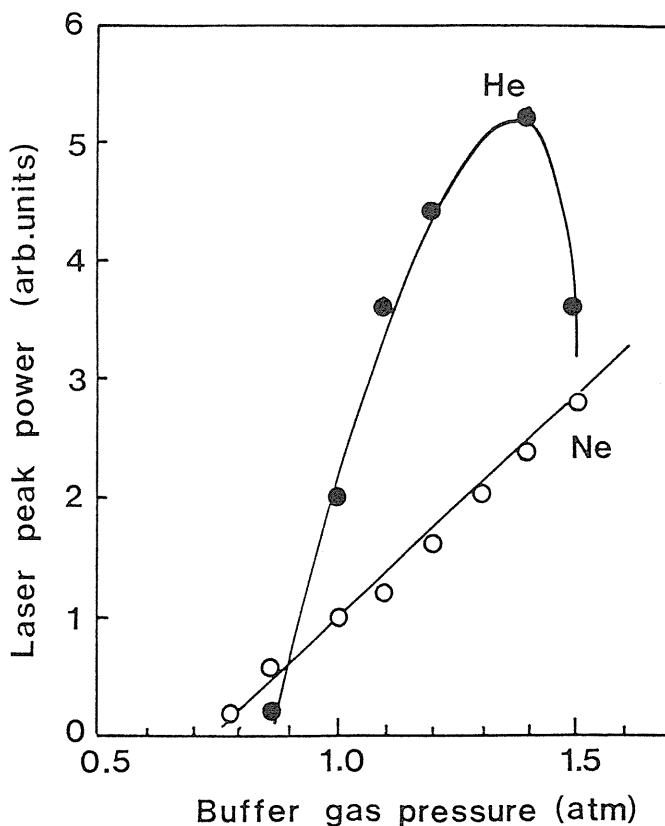
Fig. 2.8. Dependence of the laser peak power on the buffer gas pressure in the optimum gas mixtures for He and Ne buffer gases. Driving voltage 40 kV. (●): He buffer, Xe:HCl = 6 torr:2.4 torr. (○): Ne buffer, Xe:HCl = 12 torr:2.4 torr.

laser, the electric field is relatively low owing to the long electrode distance. However, high energy deposition is necessary for excimer laser performance owing to the small stimulated emission cross section.[28] On the other hand, the discharge impedance of Ne/Xe/HCl gas mixture is lower than that of He/Xe/HCl gas mixture.[30,37] Therefore, the discharge impedance of Ne/Xe/HCl gas mixture below 1.5 atm is lower than the impedance of the external excitation circuit, and the impedances do not match with each other. As a result, the energy deposition for Ne/Xe/HCl gas mixture is lower than that for He/Xe/HCl, and the gas mixture is not efficiently excited.

There is an optimum total gas pressure below 1.5 atm for He/Xe/HCl gas mixture, and there will be also an optimum gas pressure over 1.5 atm for Ne/Xe/HCl gas mixture. This is because, when the He(Ne) gas pressure is increased, the XeCl* formation increases by the three-body ion-ion recombination (2.4), but further increase causes a decrease in the electron density and reduction in the electron temperature. Besides that, the tendency of arc formation is remarkable at high gas pressures, and it results in an inhomogeneous discharge. As a result, the laser peak power decreases at high He(Ne) pressure. The difference of the optimum gas pressures for the Ne/Xe/HCl and He/Xe/HCl gas mixtures is explained by the difference of the discharge impedance. The discharge impedance of He/Xe/HCl gas mixture matches with the external excitation circuit at low pressures owing to the higher discharge impedance, but for Ne/Xe/HCl, the discharge impedance matches with the external excitation circuit at high pressures owing to the lower discharge impedance. For the compactness of the laser system, it is better to operate the laser at low gas pressure. He/Xe/HCl gas mixture is favorable for this purpose.

Figs. 2.9 show the dependences of the laser peak power on the driving voltage for various total gas pressures of Ne:Xe:HCl = 98.8:1.0:0.2 and He:Xe:HCl = 99.3:0.5:0.2. When the driving voltage is increased, the laser peak power increases and then is saturated. This driving voltage at which the laser peak power has a maximum value is higher for the higher total gas pressures. The reason of this saturation is probably because high driving voltage causes inhomogeneous discharge.
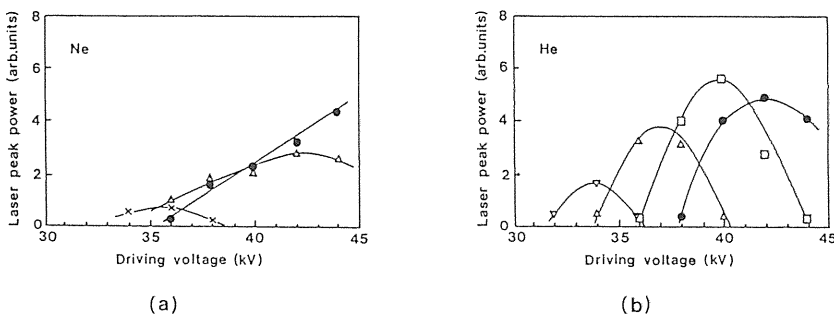

Fig. 2.9. Dependences of the laser peak powers on the driving voltage for Ne/Xe/HCl and He/Xe/HCl mixtures. Total gas pressure 1.1 atm ($\times$), 1.2 atm ($\triangledown$), 1.3 atm ($\triangle$), 1.4 atm ($\square$), 1.5 atm ($\bullet$). (a) Ne:Xe:HCl = 98.8:1.0:0.2 (b) He:Xe:HCl = 99.3:0.5:0.2.

The optimum gas mixtures have been obtained from experiments mentioned above for Ne/Xe/HCl and He/Xe/HCl gas mixtures as shown in table 2.2.

Table 2.2. Optimum concentrations of gas mixtures for Ne/Xe/HCl and He/Xe/HCl obtained from
the experiments at the driving voltage of 40 kV.

	Ne/Xe/HCl	He/Xe/HCl
Ne	›1.5 atm	—
He	—	1.3 atm
Xe	12 torr	6.0 torr
HCl	2.4 torr	2.4 torr

2.2.4.   The Other Characteristics

Fig. 2.10 shows the dependence of the laser peak power on the total gas pressure for various inner diameters of the laser tube. The driving voltage is 40 kV, and the gas mixture is He:Xe:HCl = 99.3:0.5:0.2. The inner diameter is varied from 2 to 6 mm. Highest laser peak power is obtained with a laser tube of 4 mm. The dependence of the laser peak power on the inner diameter is explained as follows. When the inner diameter is increased, the laser peak power increases owing to the increase in the discharge gas volume. However, further increase in the inner diameter causes a decrease in discharge impedance which results in a decrease in discharge voltage and electron energy. The uniformity of the discharge generally gets worse at large inner diameters also. As a result, the laser peak power decreases.
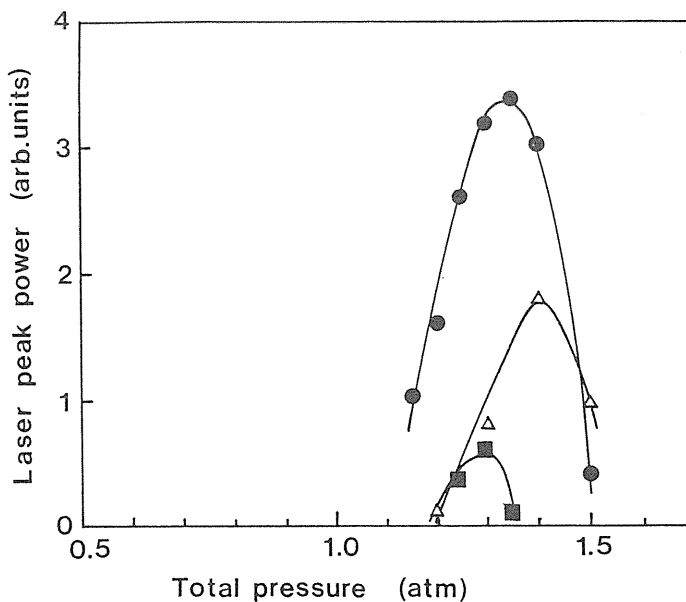

Fig. 2.10. Dependence of the laser peak power on the total gas pressure for various inner diameter of the laser tube. He:Xe:HCl = 99.3:0.5:0.2. Driving voltage 40 kV. 2 mm ($\triangle$), 4 mm ($\bullet$), 6 mm ($\blacksquare$).

Fig. 2.11 shows the dependence of the laser peak power on the output mirror reflectance at 1.3 atm of gas mixture He:Xe:HCl = 99.3:0.5:0.2. The driving voltage is 40 kV. At the output mirror reflectance of 60%, maximum laser peak power is obtained.
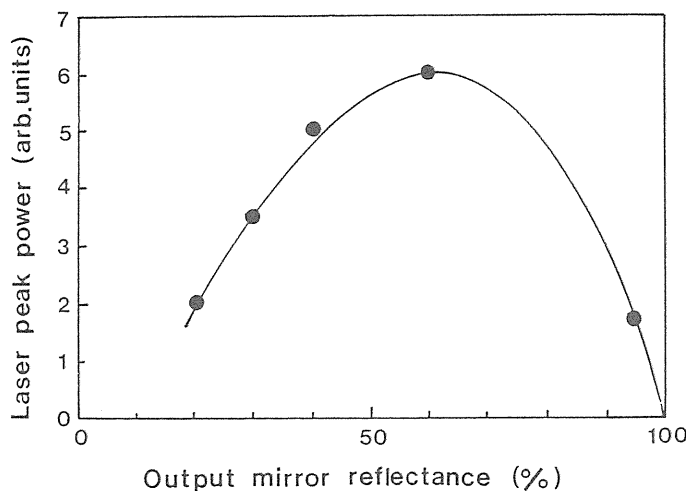
Fig. 2.11. Dependence of the laser peak power on the reflectance of the output partial reflector. Driving voltage 40 kV, He:Xe:HCl = 99.3:0.5:0.2, total gas pressure 1.3 atm.

Fig. 2.12 shows the sealed-off lifetime for three kinds of the laser tube materials at 1.3 atm of gas mixture Ne:Xe:HCl = 98.8:1.0:0.2. The driving voltage is 40 kV. When a laser tube consisting of four Teflon pipes connected to each other with five nylon pipe fittings is used, only a few tens of laser pulses are observed unless the gas mixture is replenished. Furthermore, extremely long passivation time was necessary before obtaining laser oscillation, and the shot-to-shot reproducibilities of the laser pulse energy and shape were poor. These are probably due to the decrease in HCl molecules by adsorption and reaction on nylon. When a laser tube made of all Teflon or all glass is used, the sealed-off lifetime is improved. Furthermore, the passivation time was shortened very much and the shot-to-shot reproducibilities of the laser pulse energy and shape were improved considerably. The longest sealed-off lifetime is obtained by using a Teflon laser tube.

Fig. 2.13 shows the gas-circulated lifetime for two kinds of gas mixtures Ne:Xe:HCl = 98.8:1.0:0.2, He:Xe:HCl = 99.3:0.5:0.2. of 1.3 atm. The driving voltage is 40 kV. The gas is stored in a tank of 3.8 liter and circulated by a diaphragm pump. By using gas-circulation system, the lifetime increases considerably. Furthermore, by using He/Xe/HCl gas mixture, the lifetime doubled than that of the Ne/Xe/HCl gas mixture. This is probably because the uniformity of the He/Xe/HCl discharge is better than that of Ne/Xe/HCl discharge, thus the contaminations of the former discharge are less than those of latter discharge.

The degradation of the laser power is due to the reasons as follows.[38]

(a) Deterioration of optics

A coating is deposited on the optic surfaces. This coating results from a combination of particulates, chlorocarbons, and HCl that are present inside the laser tube.
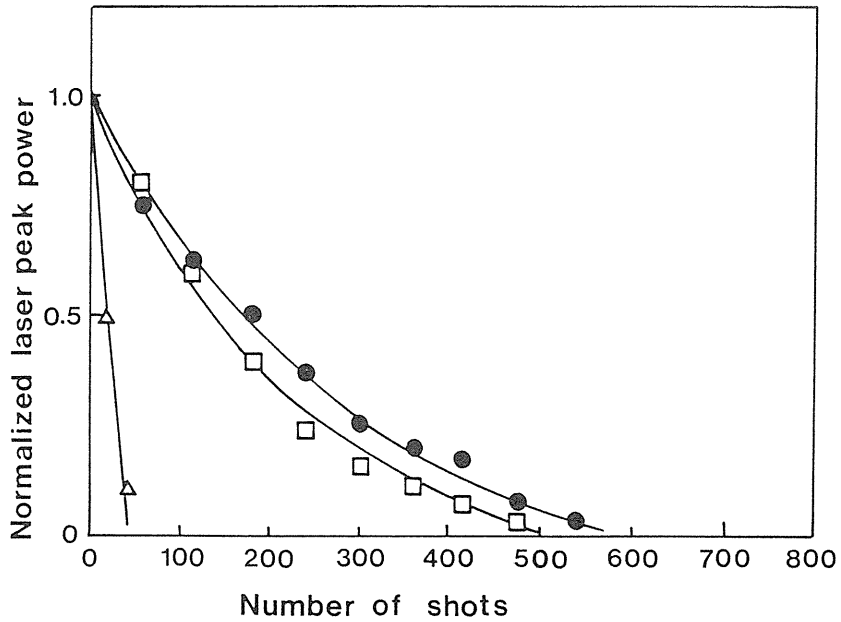
(b) Corrosion of materials

Fig. 2.12. Sealed-off lifetime of the XeCl laser for three kinds of the materials for the laser tube. Driving voltage 40 kV, Ne:Xe:HCl = 98.8:1.0:0.2, total gas pressure 1.3 atm. Nylon ($\triangle$), glass ($\square$), Teflon ($\bullet$).
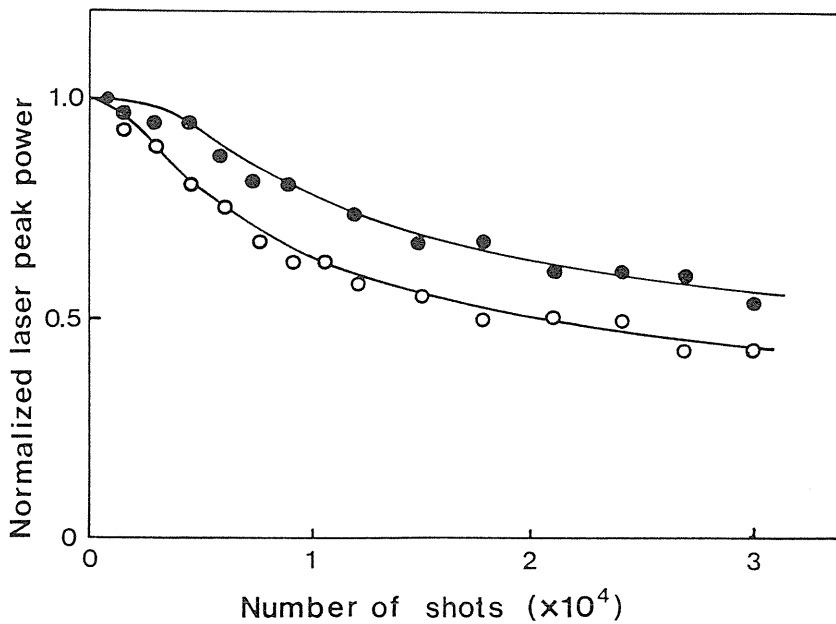

Fig. 2.13. Gas-circulated lifetime of the XeCl laser for two kinds of buffer gases. Glass tube, driving voltage 40 kV, total gas pressure 1.3 atm. Ne:Xe:HCl = 98.8:1.0:0.2 ($\bigcirc$), He:Xe:HCl = 99.3:0.5:0.2 ($\bullet$).

HCl is very corrosive, and likely to decrease by adsorption and reaction on laser parts. Especially, when the laser parts are exposed to moisture in the air, it is very corrosive.

(c)   Contamination of gas

Contaminations are mainly formed by the reaction of HCl on the laser parts (e.g. metallic chlorides). Other gaseous compounds are due to adsorption on laser parts when they are exposed to the air or chemical reactions on CO_2, H_2O, N_2 and O_2.

In this laser system, the contamination of gas or corrosion of materials is the main problem. This can be clearly seen from the fact that the initial laser performance characteristics were obtained by replenishment of the gas mixture. These problems can be solved to some extent by careful selection of laser parts, and long-term passivation. In this experiment, the longest life-time is obtained by using Teflon as shown in Fig. 2.12. This agrees with the result reported for transversal discharge XeCl excimer lasers.[38]

From a series of the experimental results shown from Fig. 2.6 to Fig. 2.13, the optimum lasing conditions for longitudinal discharge XeCl excimer laser with automatic spark UV preionization were determined to be: the total gas pressure of 1.3 atm (He:Xe:HCl = 1.3 atm: 6 torr:2.4 torr), the output mirror reflectance of 60% and inner diameter of 4 mm.

2.3.   Conclusion

Maximum laser pulse energy of about $200\,\mu J$ was obtained at the driving voltage of 40 kV. The laser pulse width was about 15 ns (FWHM). Although the output energy is smaller than that of the longitudinal discharge XeCl excimer laser reported by Zhou et al. ($317\,\mu J$ output energy, 35 ns pulse width and 30 cm discharge length)[20] because of the short discharge length, the output power per unit length is $0.5\,kW \cdot cm^{-1}$ and it is larger than that reported by them ($0.33\,kW \cdot cm^{-1}$). Furthermore, the efficiency is better than that reported by them. The laser beam spot was circular and the measured divergence was about 1 mrad (full angle), which is about five times the diffraction limit.

With a change of laser gas and a replacement of some optical components (window and external mirror), the laser device constructed in this study can be operated as the N_2 laser or other excimer lasers.

3.   Longitudinal Discharge N_2 Laser With Automatic Preionization Using LC Inversion-Charge Transfer Circuit

As mentioned in chapter 2, the spark UV preionization is useful for longitudinal discharge XeCl laser performance. However, for a longitudinal discharge N_2 laser, there was no effective preionization method. Thus, by applying the spark UV preionization method described in chapter 2 to longitudinal discharge N_2 laser, longitudinal discharge N_2 laser with automatic spark UV preionization was realized.

For obtaining a pulsed discharge UV laser of high output power, fast and uniform arc-free discharge of large current and high voltage is demanded. Therefore, a low impedance excitation circuit is necessary. In chapter 2, a charge transfer excitation circuit was used, and it was shown that the circuit is useful for obtaining a higher output power. However, since the charge of the main capacitor is not transferred 100% to the peaking capacitor for a charge-transfer circuit. The remaining charge in the main capacitor is not used effectively owing to the relatively high impedance of the main pulse generator. Thus, in this chapter, improved excitation circuit with the low impedance of the main pulse generator is proposed. It consists of the combination of a charge transfer circuit with an LC inversion circuit which is suitable

for miniaturization. The characteristics of the laser performance with the improved excitation circuit have been investigated.

Next, the characteristics of the laser output powers are interpreted qualitatively, with the excitation rate, electron density and population inversion formation rate calculated from the observed discharge voltages and currents.

Furthermore, it has been attempted to increase the laser energy by increasing the inner diameter of the discharge tube, because higher laser energy is generally expected by increasing the working volume (inner diameter). However, it has not resulted in the appreciable increase in the laser energy, and there was an optimum inner diameter. The reason for this experimental results is discussed in detail by using a computer simulation.

3.1. Experimental

A schematic diagram of the excitation scheme and a layout of the laser system used in this experiment are shown in Figs. 3.1 and 3.2. The laser system is the same as that described in chapter 2 except the main pulse generator, the resonator and the peaking capacitor C_0. The optical resonator is not composed, because the population inversion ends in a very short time owing to the short lifetime of the laser transition. One aluminum coated mirror with 100% reflection is used for the purpose of increasing the output power and decreasing the divergence of the laser beam. The capacitance of the peaking capacitors C_0, C_1 and C_2 are 150 pF, 1700 pF and 1700 pF, respectively. In stead of the two-stage Marx bank generator, an LC inversion circuit is used as the main pulse generator. When the spark gap switch is closed, a voltage inversion of the capacitor C_2 occurs owing to the inductance composed of the spark gap switch and capacitor C_2, and a rapidly rising high-voltage pulse is applied to the laser tube. The methods of the observations of laser pulse energies, laser pulse shapes, currents, and voltages are also the same as those described in chapter 2.
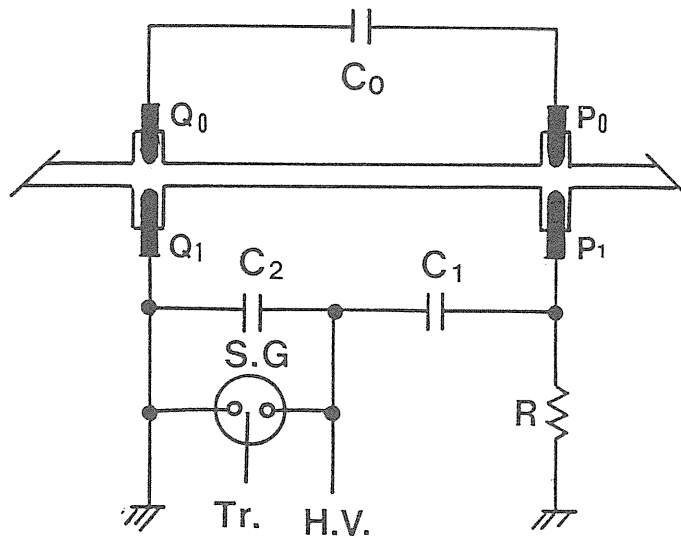

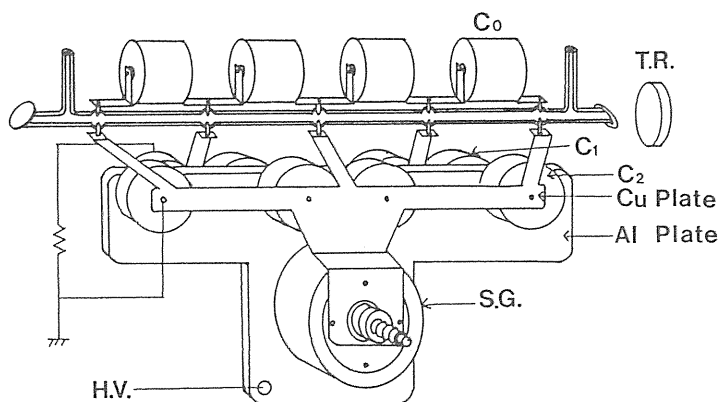Fig. 3.1. Schematic diagram of the excitation scheme. S.G.: spark gap, Tr.: trigger.

Fig. 3.2. Layout of the laser system. T.R.: total reflector. $C_0 = 150$ pF, $C_1 = C_2 = 1700$ pF, R = 3 kΩ.

3.2. Results and Discussion

3.2.1. Comparison of the Laser Output Performances of the N_2 Lasers Using LC Inversion—Charge Transfer Circuit and Marx Bank—Charge Transfer Circuit

The impedance of the LC inversion circuit composed of the capacitor C_2 and the spark gap switch has been estimated by comparing open-circuit voltage waveforms (the peaking capacitors were not connected) with those calculated by using an equivalent circuit. The impedance of the spark gap switch was assumed to be time-independent for simplicity. The estimated resistance and inductance are about 0.35 Ω and 25 nH, respectively. The observed voltage rising time is about 50 ns, and the peak voltage is about 1.6 times as high as the charging voltage.

Fig. 3.3 shows the time behavior of the voltage pulse V_0 between P_0 and Q_0, V_1 between P_1 and Q_1, the current I_0 from the capacitor C_0, I_1 from the capacitor C_1, the longitudinal discharge current I_2, and the 337 nm N_2 laser pulse. The charging voltage is 20 kV and the N_2 gas pressure is 60 torr. About 40 ns after the turn-on of the spark gap switch, spark UV preionization (I_1, I_0) occurs between P_1–P_0 and between Q_1–Q_0. About 20 ns after the start of the spark UV preionization, the longitudinal discharge (I_2) occurs and the 337 nm N_2 laser pulse with a width of about 5 ns (FWHM) is obtained. The peak voltage between P_0 and Q_0 is higher than that between P_1 and Q_1. This is because the small gaps P_0–P_1 and Q_0–Q_1 act as self-triggered spark gap switches, and thus enhance the peaking effect of capacitor C_0. In the case of two-stage Marx bank generator, such an effect was not observed because of the high impedance of the spark gap switches. At the beginning of the longitudinal discharge in the case of the LC inversion pulse generator, current I_0 from the capacitor C_0 is large, and current I_1 from the capacitor C_1 increases later on.

The characteristics of the laser ouput power and the discharge parameters obtained using an LC inversion—charge transfer excitation circuit (type II) are compared with those using only a charge transfer excitation circuit with a two-stage Marx bank generator (type I). The excitation circuits are shown in Figs. 3.4 (a) and (b). Fig. 3.5 shows the dependence of the laser peak power on the N_2 gas pressure for the type I and type II lasers. The charging voltage is 20 kV. The maximum laser peak powers of the type I and type II lasers are about 52 kW and 65 kW, respectively, and the pulse width for both is about 5 ns (FWHM). Thus the output power of the type II laser is 25% higher than that of the type I laser.
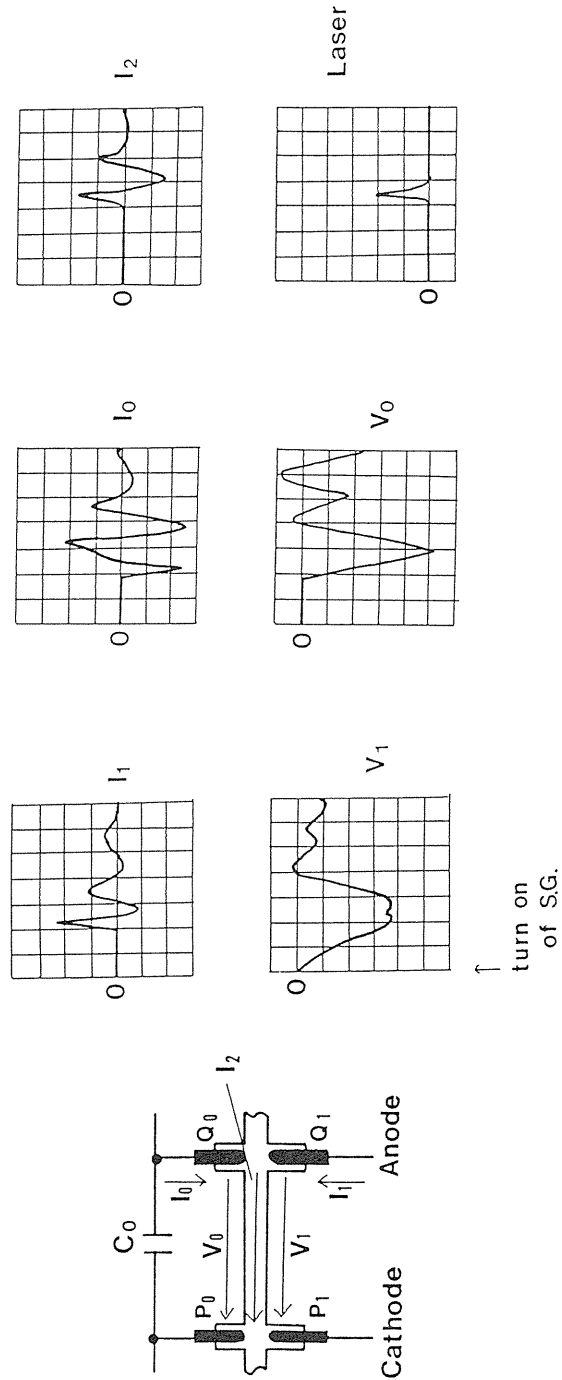
Fig. 3.3. Time behaviors of the waveforms. Discharge voltage, current, and laser pulse (337 nm). Gas
pressure 60 torr, charging voltage 20 kV. Horizontal axis: 20 ns/div. Vertical axis: arbitrary
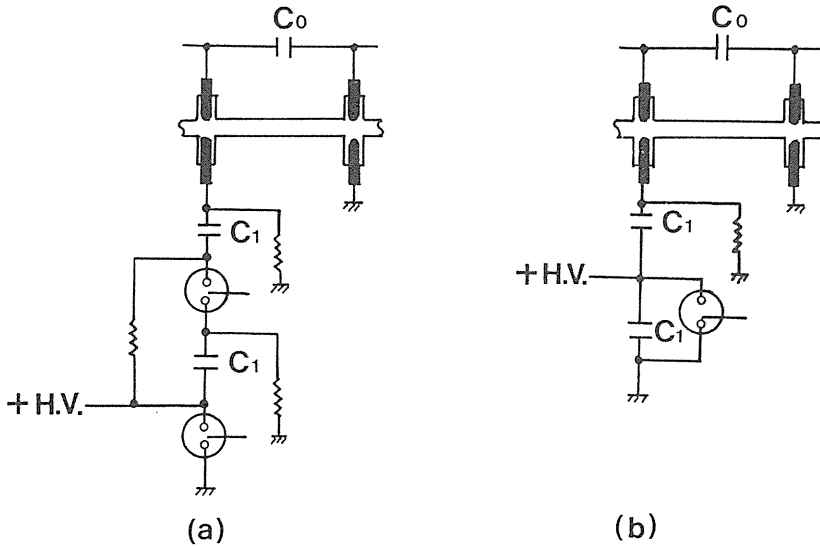units.

Fig. 3.4. Two types of the excitation circuit. (a) Type I; charge transfer excitation circuit with two-stage Marx bank generator, (b) type II; LC inversion-charge transfer excitation circuit.
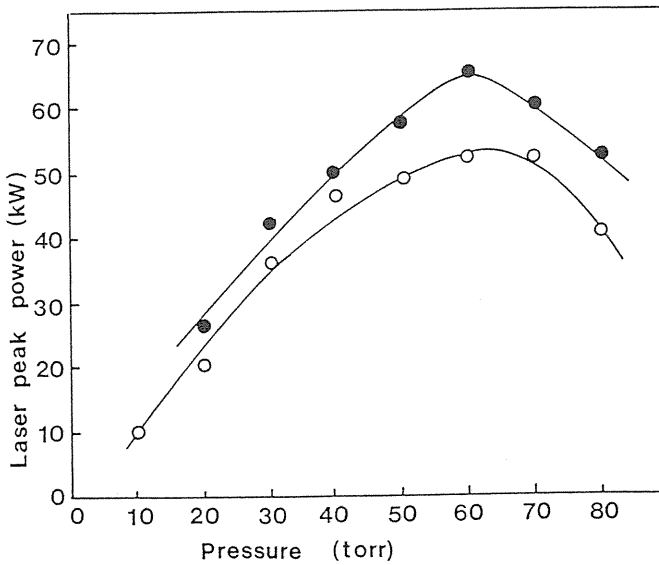

Fig. 3.5. Dependence of the laser peak power on the gas pressure for the two types of excitation circuits. Charging voltage 20 kV. Type I laser ($\bigcirc$), type II laser ($\bullet$).

Fig. 3.6 shows the dependence of the breakdown voltage on the gas pressure for the two types of excitation circuits shown in Fig. 3.4. The charging voltage is 20 kV. For the type II laser, the average of the breakdown voltages between P_0 and Q_0 and between P_1 and Q_1 is used as the breakdown voltage, because these two voltages are different from each other. The
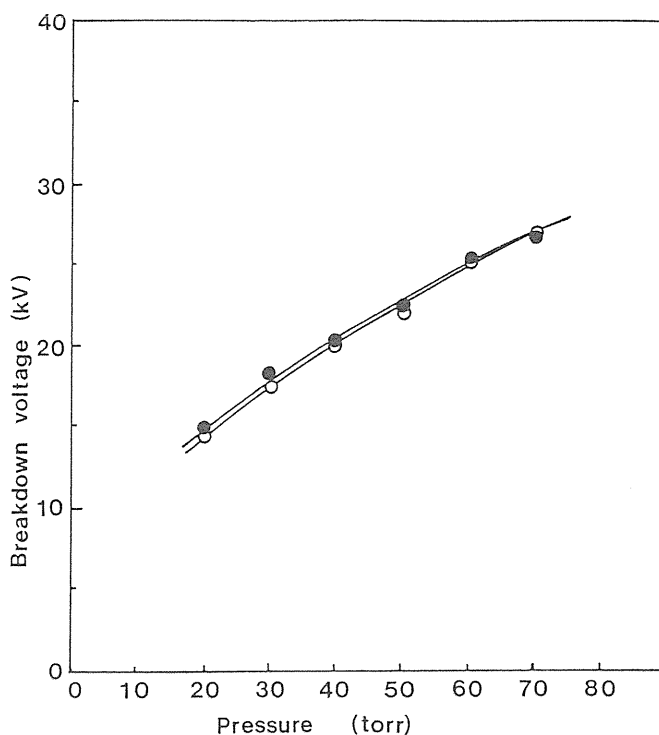
Fig. 3.6. Dependence of the breakdown voltage on the gas pressure for the two types of excitation circuits. Charging voltage 20 kV. Type I laser (○), type II laser (●).

breakdown voltages do not differ so much with the two types of the lasers. Fig. 3.7 shows the dependence of the discharge peak current I_2 on the gas pressure for the two types of excitation circuits shown in Fig. 3.4. The charging voltage is 20 kV. The discharge peak current of the type II laser is larger than that of the type I laser, especially at low pressures.

Fig. 3.8 shows the dependence of the laser peak power on the charging voltage for the type I and type II lasers shown in Fig. 3.4. The N_2 gas pressure is 60 torr. The threshold voltage of the type I laser is lower than that of the type II laser. This is because the open-circuit voltage of the LC inversion pulse generator is about 1.6 times as high as the charging voltage, while that of the type I pulse generator is about 2 times as high as the charging voltage. However, the laser peak power of the type II laser is higher than that of the type I laser at the charging voltages above 18 kV because of the low impedance of the excitation circuit.

Fig. 3.9 shows the dependence of the breakdown voltage on the charging voltage for the two types of the excitation circuits shown in Fig. 3.4. The gas pressure is 60 torr. At high charging voltage, the breakdown voltages do not differ so much with the two types of the lasers, but at low charging voltage, the breakdown voltage of the type II laser is slightly low. Fig. 3.10 shows the dependence of the discharge peak current I_2 on the charging voltage for the two types of excitation circuits shown in Fig. 3.4. The gas pressure is 60 torr. The discharge peak current of the type II laser is slightly larger than that of the type I laser.

As shown above, the laser peak power of the N_2 laser using an LC—inversion charge transfer excitation circuit is about 25% higher than that using a charge transfer excitation
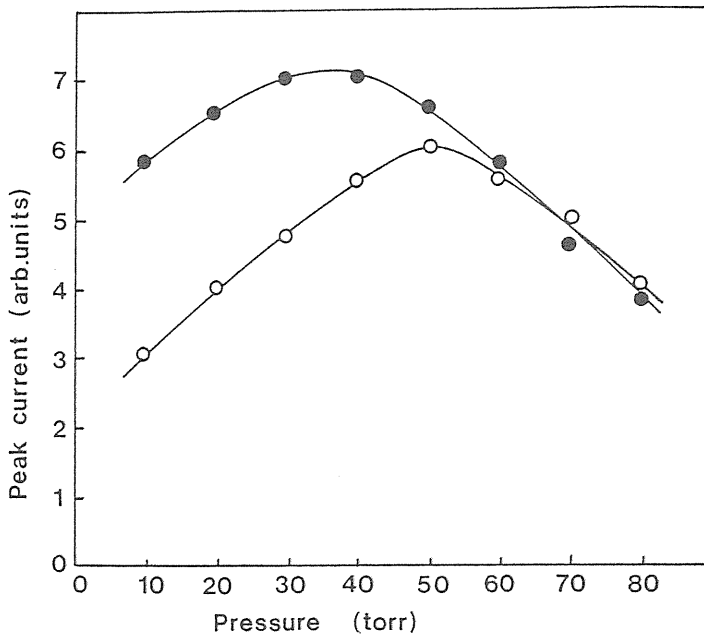
Fig. 3.7. Dependence of the peak current on the gas pressure for the two types of excitation circuits. Charging voltage 20 kV. Type I laser (○), type II laser (●).
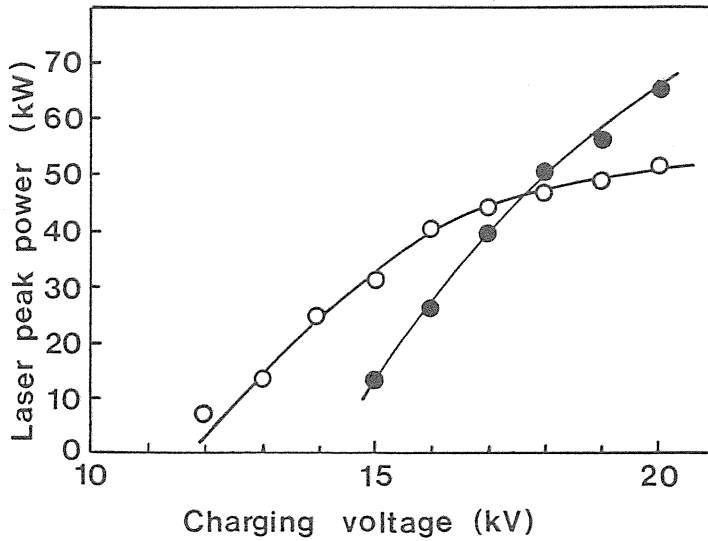

Fig. 3.8. Dependence of the laser peak power on the charging voltage for the two types of excitation circuits. Gas pressure 60 torr. Type I laser (○), type II laser (●).
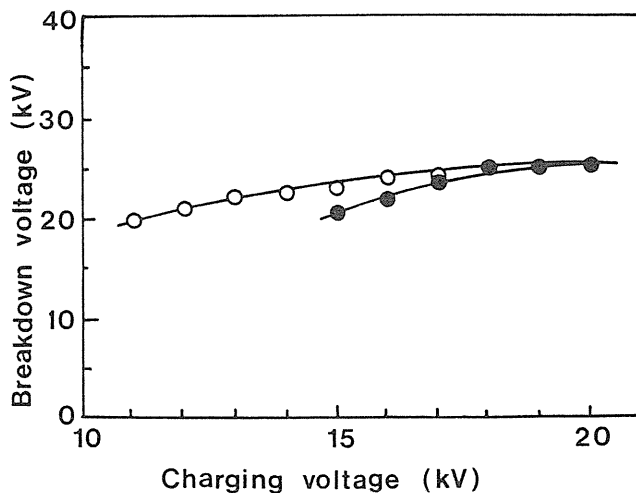
Fig. 3.9. Dependence of the breakdown voltage on the charging voltage for the two types of excitation circuits. Gas pressure 60 torr. Type I laser (○), type II laser (●).
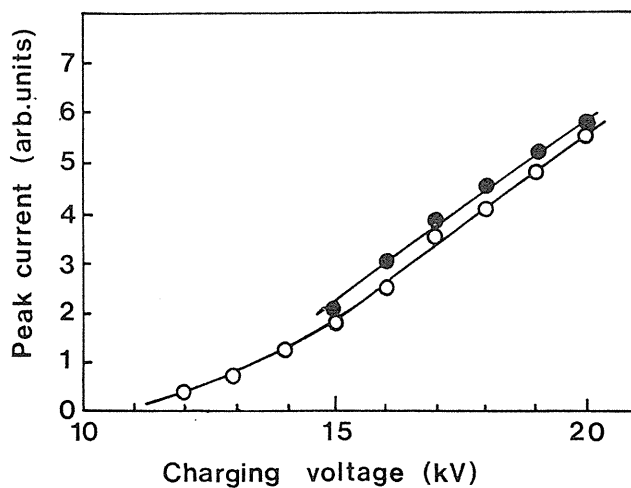

Fig. 3.10. Dependence of the peak current on the charging voltage for the two types of excitation circuits. Gas pressure 60 torr. Type I laser (○),type II laser (●).

circuit with a two-stage Marx bank generator at the charging voltage of 20 kV owing to the increase in the discharge current. Furthermore, N_2 laser using the LC inversion—charge transfer excitation circuit is simpler than that using two-stage Marx bank generator. Therefore, this excitation technique is favorable for the compactness of the N_2 laser.

3.2.2. Qualitative Interpretation of the Characteristics of the Laser Peak Power Using Spark UV Preionization

The three types of excitation circuits shown in Fig. 2.5 were used for investigating the effects of the spark UV preionization and the charge transfer circuit. The main pulse generator for applying high voltage pulses between electrode pins P_1 and Q_1 is an LC inversion pulse generator. The first type laser has been operated without the spark UV preionization or peaking capacitor C_0 (type 1); the second has been operated without the sprak UV preionization but by connecting the peaking capacitor C_0 between the electrode pins P_1 and Q_1 (type 2); the third has been operated with the spark UV preionization and by connecting the peaking capacitor C_0 between the electrode pins P_0 and Q_0 (type 3).

Fig. 3.11 shows the dependence of the laser peak power on the N_2 gas pressure for the three types of excitation circuits shown in Fig. 2.5. The charging voltage is 20 kV. Although the maximum peak power of the type 1 laser is about 37 kW, that of the type 2 laser is about 50 kW. Furthermore, the maximum laser peak power of about 65 kW is obtained with the type 3 laser. In each case, there is an optimum pressure at which the laser peak power is maximum. The optimum pressure for the type 3 laser is about 60 torr, whereas it is 30 torr for both the type 1 and 2 lasers.
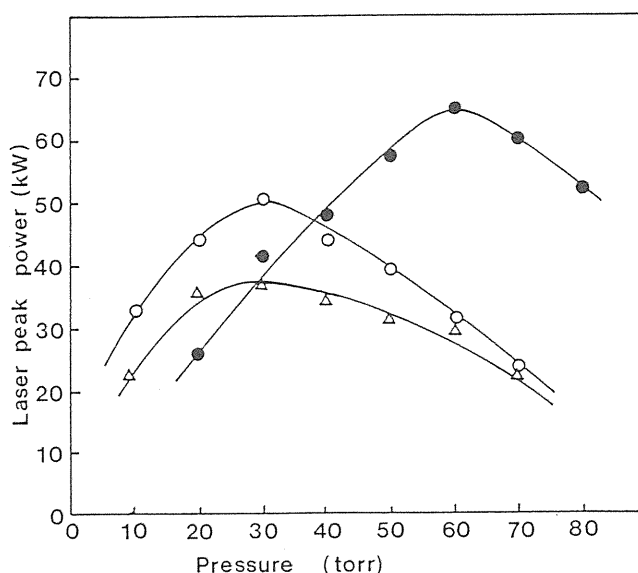

Fig. 3.11. Dependence of the laser peak power on the gas pressure for the three types of excitation circuits. Charging voltage 20 kV. Type 1 laser ($\triangle$), type 2 laser ($\bigcirc$), type 3 laser ($\bullet$).

Fig. 3.12 shows the dependence of the laser peak power on the charging voltage for the three types of excitation circuits shown in Fig. 2.5. The N_2 gas pressure is 60 torr. When the type 3 laser is used, maximum laser peak power is obtained, and the laser peak power of the type 2 laser is higher than that of the type 1 laser. Furthermore, the threshold voltage of the type 3 laser is the lowest, and that of the type 2 laser is lower than that of the type 1 laser.

The sealed-off lifetime was investigated for the three types of excitation circuits shown in Fig. 2.5 at the N_2 gas pressure of 30 torr, charging voltage of 20 kV and repetition rate of
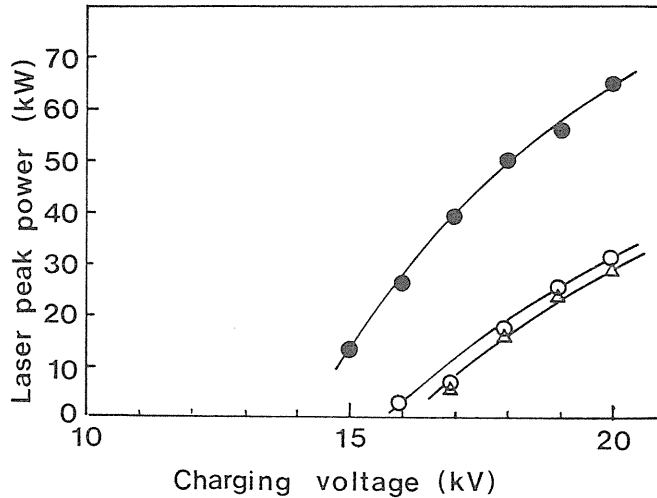
Fig. 3.12. Dependence of the laser peak power on the charging voltage for the three types of excitation circuits. Gas pressure 60 torr. Type 1 laser ($\triangle$), type 2 laser ($\bigcirc$), type 3 laser ($\bullet$).

10 pps. The numbers of shots at which the laser peak power decreased to 90% of the initial value for type 1, 2 and 3 lasers were about 0.5×10^5, 1.0×10^5 and 1.5×10^5, respectively. The decrease of the laser peak power was probably due to impurities from the laser tube or electrodes, because the initial laser performance characteristics were obtained by the replenishment of the N_2 gas.

The shot-to-shot reproducibility of the laser peak power was measured with the three types of excitation circuits shown in Fig. 2.5 at the N_2 gas pressure of 30 torr and charging voltage of 20 kV. The reproducibility of the type 1 laser was $\pm 50\%$. However, that of the type 2 laser was $\pm 20\%$ and that of the type 3 laser was $\pm 5\%$. This is probably because the shot-to-shot reproducibility of the breakdown voltage is improved by using the spark UV preionization and the charge transfer circuit. That is, the difference of the time lags of the breakdown between the four segment is decreased and the discharge uniformity is improved by using these techniques.

These results show that the charge transfer circuit and the spark UV preionization are effective for increasing the laser peak power and improving the sealed-off lifetime of the laser operation and shot-to-shot reproducibility of longitudinal discharge low-pressure N_2 laser.

Fig. 3.13 shows the dependence of the breakdown voltage on the N_2 gas pressure for the three types of excitation circuits shown in Fig. 2.5. The charging voltage is 20 kV. The breakdown voltage of the type 3 laser changes with the N_2 gas pressure more considerably than those of the other two types of lasers. This is because at high N_2 gas pressures, the peaking capacitor C_0 heightens the breakdown voltage by the peaking effect, although at low N_2 gas pressure a remarkable peaking effect does not appear because of the low breakdown voltage of the small gaps for the spark UV preionization.

Fig. 3.14 shows the dependence of the discharge peak current I_2 on the N_2 gas pressure for the three types of excitation circuits shown in Fig. 2.5. The charging voltage is 20 kV. At high gas pressure, the peak current of the type 3 laser is larger than those of the type 1 and 2 lasers owing to the spark UV preionization and the high discharge voltage. It is noticed that

with an increase in N_2 gas pressure, the discharge peak currents of the type 1 and 2 lasers decrease, but that of the type 3 laser shows a maximum at about 40 torr.

Next, the electron density and excitation rate coefficient have been calculated from the observed discharge voltage and current. For the low pressure N_2 laser, neither collisions between molecules nor ion-electron recombination can be important during the first stage of the discharge, and the direct electron impact excitation process from the ground state $X^1\Sigma_g^+$ (v'' = 0) to the $C^3\Pi_u$ (v' = 0) and $B^3\Pi_g$ (v' = 0) states of N_2 discharge is the dominant one.[39]
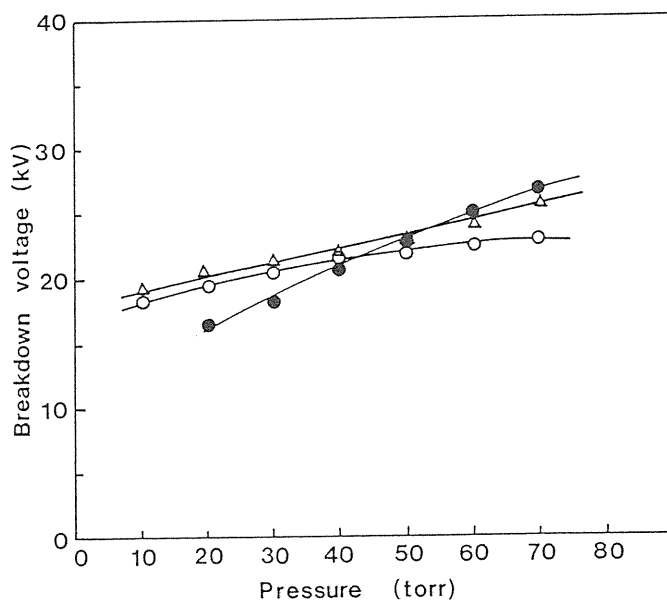
Fig. 3.13. Dependence of the breakdown voltage on the gas pressure for the three types of excitation circuits. Charging voltage 20 kV. Type 1 laser ($\triangle$), type 2 laser ($\bigcirc$), type 3 laser ($\bullet$).
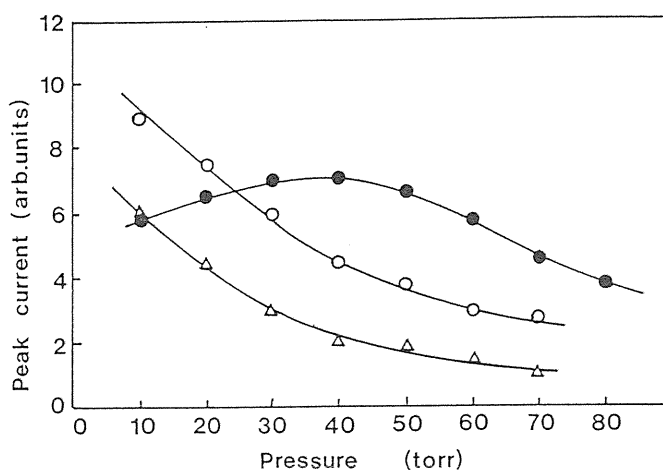
Fig. 3.14. Dependence of the peak current on the gas pressure for the three types of excitation circuits. Charging voltage 20 kV. Type 1 laser ($\triangle$), type 2 laser ($\bigcirc$), type 3 laser ($\bullet$).

The excitation rate P_j to the j state from the ground state by electron impact is given by

$$P_j = N_x N_e X_j \qquad (3.1)$$

Here N_x is the density of molecules in the ground state which is known simply from the N_2 gas pressure. N_e is the electron density and X_j is the excitation rate coefficients from the ground state to the j state. These X_j and N_e are estimated in the following way.

The excitation rate coefficient X_j is given by

$$X_j = \int \sigma_j(\varepsilon) v_e(\varepsilon) f(\varepsilon) d\varepsilon$$

$$= \int \sigma_j(\varepsilon) \sqrt{\frac{2\varepsilon}{m_e}} f(\varepsilon) d\varepsilon \qquad (3.2)$$

Here v_e, m_e ε and σ_j are the electron velocity, the mass of an electron, the kinetic energy of the electron, and the excitation cross section to the j state, respectively. $f(\varepsilon)$ is the electron energy distribution function, which is assumed to be approximately Maxwellian at E/P values above 30 Vcm^{-1}torr^{-1} (E is the electric field, P is the N_2 gas pressure).[39] This excitation rate coefficient was calculated by Cartwright as a function of the electron temperature.[40] Furthermore the E/P and electron temperature T_e in the N_2 gas discharge are related approximately by[39]

$$kT_e = 0.11 \cdot E^{0.8} \cdot P^{-0.8} \text{ (eV)} \qquad (3.3)$$

Here k is the Boltzmann constant. Thus we can calculate the excitation rate coefficient X_j by using the observed electric field (discharge voltage) and the N_2 gas pressure.

Fig. 3.15 shows the dependence of the difference $X_c - X_b$ of the peak excitation rate coefficients of the $C^3\Pi_u(v' = 0)$ and $B^3\Pi_g(v' = 0)$ states on the N_2 gas pressure for the three types of the excitation circuits shown in Fig. 2.5. The charging voltage is 20 kV. The published data by Benesch et al.[41] were used as the Franck-Condon factors for electron excitation of the $v' = 0$ vibration levels in the $C^3\Pi_u$ and $B^3\Pi_g$ states connecting with the $v'' = 0$ vibration level in the $X^1\Sigma_g^+$ ground state.[41] At low N_2 gas pressures, the $X_c - X_b$ of the type 3 laser is rather small compared with the other two owing to the lower breakdown voltage. With an increase in N_2 gas pressure, the $X_c - X_b$ of any type of laser decreases owing to the decrease in the electron temperatures.

The electron density N_e is obtained from the following relation using the measured discharge current.

$$N_e = I \cdot (\pi \cdot r^2 \cdot e \cdot v_d)^{-1} \qquad (3.4)$$

Here I, r, e, and v_d are the discharge current, the tube radius, the electronic charge, and the electron drift velocity, respectively. The electron drift velocity v_d is calculated from[42),43]

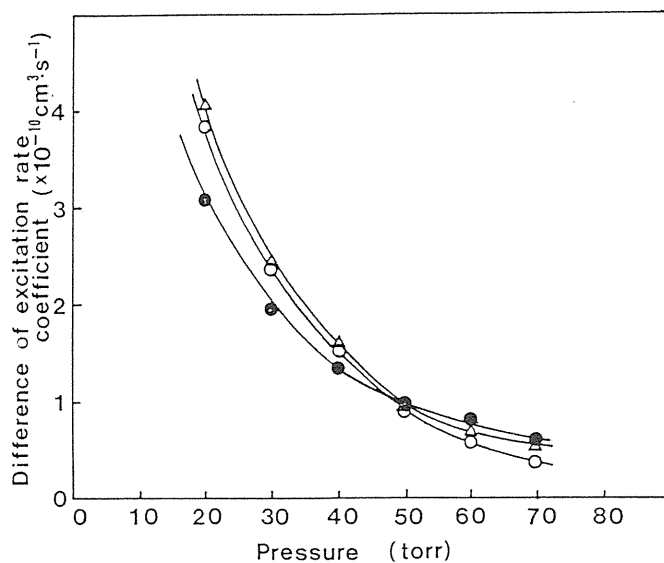$$v_d = 2.9 \times 10^5 \cdot E \cdot P^{-1} \text{ (cm} \cdot \text{s}^{-1}) \qquad (3.5)$$

Fig. 3.15. Dependence of the difference of the excitation rate coefficient on the gas pressure for the three types of excitation circuits. Charging voltage 20 kV. Type 1 laser ($\triangle$), type 2 laser ($\bigcirc$), type 3 laser ($\bullet$).

Fig. 3.16 shows the dependence of the peak electron density N_e (relative) on the N_2 gas pressure for the three types of excitation circuits shown in Fig. 2.5. The charging voltage is 20 kV. The peak electron density of the type 2 laser is larger than that of the type 1 laser, because the peak current of the type 2 laser is larger than that of the type 1 laser, and the E/P
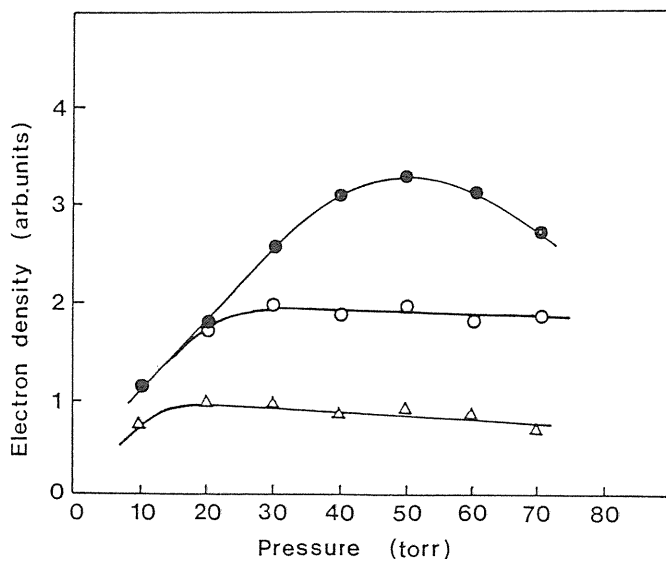

Fig. 3.16. Dependence of the peak electron density Ne on the gas pressure for the three types of excitation circuits. Charging voltage 20 kV. Type 1 laser ($\triangle$), type 2 laser ($\bigcirc$), type 3 laser ($\bullet$).

values of the type 2 and type 1 lasers do not differ so much. Furthermore, the peak electron density of the type 3 laser is larger than those of the other two types of lasers, especially at high N_2 gas pressures. This is due to the effect of the spark UV preionization which increases the initial electrons and improves the discharge uniformity, and the effect of the peaking capacitor C_0.

While the peak electron densities of the types 1 and 2 lasers are saturated at 20 torr ~ 30 torr, that of the type 3 laser increases up to about 50 torr. This is because the spark UV preionization is more effective at high pressures, and the increase in the discharge voltage with the N_2 gas pressure is more considerable than those of the other two types of lasers.

Fig. 3.17 shows the dependence of the calculated population inversion formation rate $P_c - P_b$ on the N_2 gas pressure for the three types of excitation circuits shown in Fig. 2.5. The charging voltage is 20 kV. Here P_c and P_b are the peak excitation rate to the $C^3 \Pi_u (v' = 0)$ and $B^3 \Pi_g (v' = 0)$ states by electron impact, respectively. The deexcitations by the collisional mixing of the laser levels are not included. These calculated $P_c - P_b$ explain the N_2 gas pressure dependence of the peak laser output powers shown in Fig. 3.11 qualitatively well.

From these considerations, we may conclude the following. First, the increase in laser peak power with the charge transfer circuit and spark UV preionization are mainly due to the increase in electron density. Second, the higher N_2 gas pressure at which maximum laser peak power is obtained with the type 3 laser is due to the higher N_2 gas pressure at which maximum electron density is obtained.

3.2.3. Optimization of the Inner Diameter of the Discharge Tube

Fig. 3.18 shows the dependence of the laser peak output power on the N_2 gas pressure for the three types of laser tubes with different inner diameters at the charging voltage of 20 kV. The pulse width (FWHM) was 5 ns for each type. The working volume increases with the square of the inner diameter of the discharge tube. However, the output power per unit volume decreases with the inner diameter. Therefore, there is an optimum inner diameter for the output power. In this experiment, for the three types of lasers with 2, 4, and 6 mm inner diameters, the maximum laser peak output powers are 23, 65, and 40 kW, and maximum laser output energies per unit volume are 0.23, 0.10, and 0.017 mJ · cm^{-3}, respectively. The optimum inner diameter is 4 mm.

The main reason for the decrease in the laser output power per unit volume is not clear, but some reasons are considered. First, when the inner diameter is increased, the impedance of the discharge decreases owing to the increase in the discharge cross-section. It causes a decrease in the discharge voltage. As a result, the electron energy falls, and the excitation rate lowers. It also agrees with the result that the optimum pressure is lowered when the inner diameter is increased.

However, it is worth mentioning that concentration of the discharge near discharge tube wall region by the skin depth effect occurs in a discharge tube of several mm inner diameter with a several ns pulsed discharge. A detailed discussion has been made by using computer simulation.

The same excitation processes described in section 3.2.2 are assumed. The discharge parameters are radial and temporal variables in the system of equations.

The governing equation for the electron density N_e is

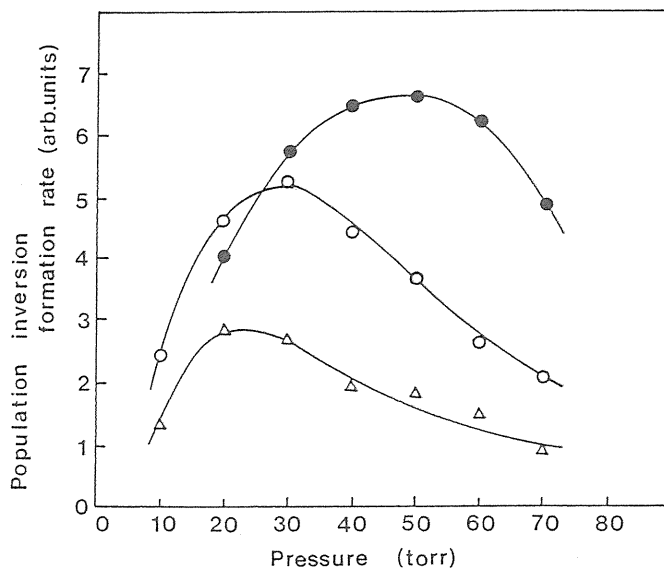$$\frac{dN_e}{dt} = \alpha \cdot v_d \cdot N_e \tag{3.6}$$

Fig. 3.17. Dependence of the population inversion formation rate on the gas pressure for the three types of excitation circuits. Charging voltage 20 kV. Type 1 laser ($\triangle$), type 2 laser ($\bigcirc$), type 3 laser ($\bullet$).
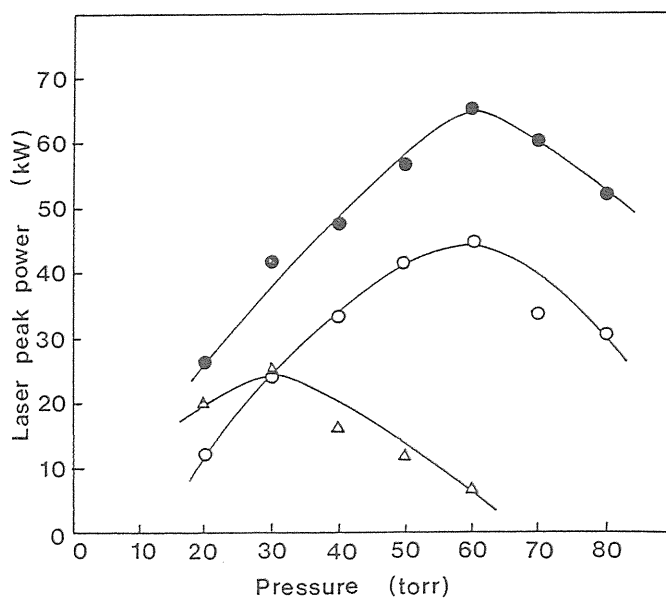

Fig. 3.18. Dependence of the laser peak power on the gas pressure for the circular cross-section laser for the discharge tubes of 2 ($\bigcirc$), 4 ($\bullet$) and 8 mm ($\triangle$) inner diameter. Charging voltage is 20 kV.

convective transport of electrons is neglected, because it is very slow compared with the pulsed discharge width. Here α is the ionization coefficient, and simply calculated from[42),43)]

$$\alpha = 1.4 \times 10^{-8} \cdot E^{3.7} \cdot P^{-2.7} \ (\text{torr}^{-1} \cdot \text{cm}^{-1}) \tag{3.7}$$

Here E and P are the electric field and N_2 gas pressure, respectively. v_d is the drift velocity and calculated from the equation (3.5). The conductivity is calculated from

$$\sigma = e \cdot N_e \cdot v_d \cdot E^{-1} \tag{3.8}$$

Here e is the electronic charge.

The resultant longitudinal electric field is described by a diffusion-like equation:

$$\nabla^2 \cdot E = \mu_0 \frac{\mathrm{d}(\sigma \cdot E)}{\mathrm{d}t} \tag{3.9}$$

The excitation rate coefficients are calculated from the equations (3.2). These parameters are radial and temporal variables in the system of equations.

Fig. 3.19 shows the equivalent discharge circuit. The values of the parameters were determined from the observed voltages and currents at some point of the circuit. S_g is the spark gap switch and Z is the discharge impedance. The discharge tube of 4 mm inner diameter and 65 mm discharge length with 50 torr N_2 gas pressure is considered. S_p is the spark UV preionization gap which is closed when the applied voltage reaches 20 kV. The initial electron density of $1 \times 10^{11} \ \text{cm}^{-3}$ is assumed (it does not influence the result very much) and the breakdown initiated by multiple primary avalanches is assumed.

The computed longitudinal electric field as a function of radius after the start of the discharge is shown in Fig. 3.20. The electric field decreases at the center of the discharge tube rather than near the tube wall. The decrease of the electric field is slight, but ionization coef-
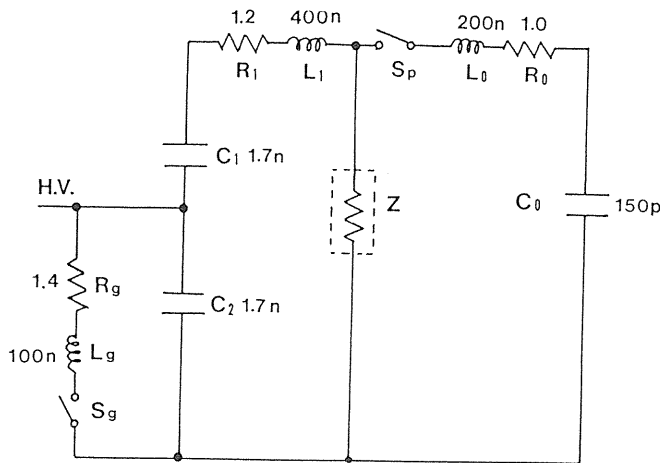

Fig. 3.19. Laser discharge circuit. S_g: spark gap switch, S_p: preionization gap. Z: discharge impedance (length 65 mm, inner diameter 2 mm).

ficient is in proportion to $E^{3.7}$. Therefore it causes a large delay of the ionization, and the electron density at the center of the discharge tube increases slowly.

Fig. 3.21 shows the computed electron density as a function of radius after the start of the discharge. The discharge concentrates near the tube wall owing to the skin depth effect. Normally, at the electron density $N_e > 6 \times 10^{14}\,\mathrm{cm}^{-3}$, the collisional mixing of the laser levels by electron impact becomes dominant and the laser pulse width is shortened compared with the radiative lifetime of the upper laser level of 40 ns.[44] In this result, the electron density reaches to $6 \times 10^{14}\,\mathrm{cm}^{-3}$ at 6–8 ns after the start of the discharge. This agrees with the result that the laser pulse terminates at 10 ns after the start of the discharge.

As the results, it was proved that the skin depth effect may occur in the discharge tube of this laser system. Therefore, the center of the discharge tube is not efficiently excited. Laser beams in the shape of a hollow cylinder have been actually reported on pulsed discharge lasers with a circular cross-section.[45] It is expected that higher laser energy is obtained if the skin depth effect can be avoided.
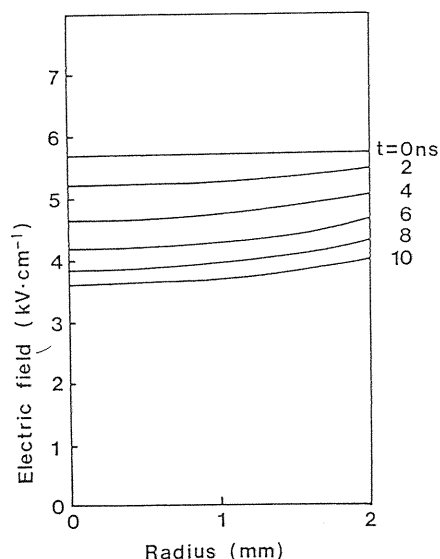

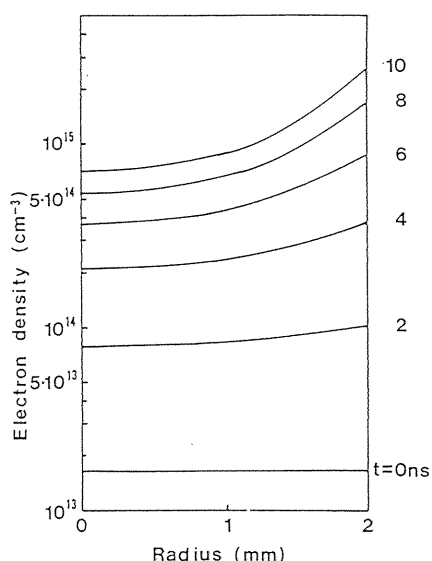Fig. 3.20. Computed electric field as a function of radius after the start of the discharge.

Fig. 3.21. Computed electron density as a function of radius after the start of the discharge.

3.3. Conclusion

A longitudinal discharge low pressure N_2 laser with automatic spark UV preionization has been developed. The laser performance was improved considerably by using spark UV preionization, LC inversion circuit, and charge transfer circuit. The excitation rate, electron density and population inversion formation rate were calculated, and it was concluded that the improvement of the laser performance with automatic spark UV preionization and charge transfer circuit is mainly due to the high electron density.

There was an optimum inner diameter of the discharge tube. The reason for the decrease in the laser output power at large inner diameter was discussed by using a computer simula-

tion. It has been proved that skin depth effect affects the discharge and excitation of the N_2 molecules in this type of discharge tube. If it is possible to increase the working volume without skin depth effect, higher laser energy is expected.

4. Longitudinal Discharge N_2 Laser with Rectangular Cross-Section

As discussed in chapter 3, when the working volume, is increased by increasing the inner diameter of the circular cross-section discharge tube, the laser energy is not increased owing to the skin depth effects. Thus, in this chapter, a longitudinal discharge N_2 laser with a rectangular cross-section of large working volume has been realized to increase the laser output energy.

4.1. Experimental

Fig. 4.1 shows the laser tube structure of the rectangular cross-section laser. The electrical circuit is the same as that of the circular cross-section laser described in chapter 3 except peaking capacitors. The capacitance of the peaking capacitor C_0 is 560 pF. The laser tube employs a four-segmented longitudinal discharge chamber with a rectangular cross-section. The chamber is made of Pyrex-Glass plates which are glued with an adhesive. The total length of the discharge is the same as that of the circular cross-section laser described in chapter 3. The wall gap (H) is 2 mm and the tube width (W) is 20 mm. The electrodes widths are the same as the tube width, and they have saw-toothed surface to obtain uniform preionization and discharge.
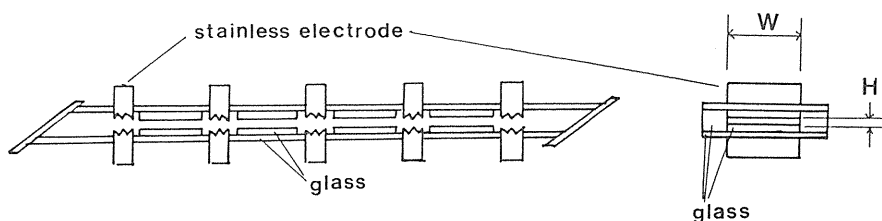

Fig. 4.1. Laser tube structure of the rectangular cross-section laser.

4.2. Results and Discussion

4.2.1. Characteristics of the Laser System

Fig. 4.2 shows the dependence of the laser peak power on the number of the discharge segments. The charging voltage is 20 kV, and the gas pressure is 30 torr. The discharge length of the one segment is 6.5 cm. Since a total reflector was used at one side, one segment corresponds to an active length of 13 cm. From this result for a short discharge length, the gain is estimated to be approximately $65 \, dB \cdot m^{-1}$. For long discharge lengths, the power saturates and approaches linear increase with the length. Thus the saturation power is estimated to be approximately $7.5 \, kW \cdot cm^{-3}$. These values are typical of transversal discharge low pressure N_2 lasers.[46] The loss of the power in the discharge tube and the coupling loss were neglected

in this calculation, and the real power gain and saturation power are larger than the values mentioned above.
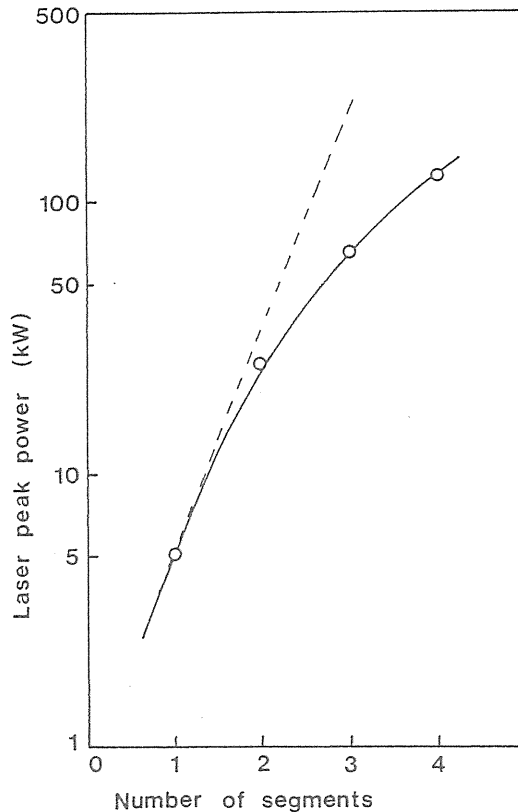

Fig. 4.2. Dependence of the laser peak power on the number of the discharge segment. Charging voltage: 20 kV. Gas pressure 30 torr. One segment corresponds to an active length of 13 cm.

Fig. 4.3 shows the dependence of the laser peak power on the peaking capacitor. The charging voltage is 20 kV and the gas pressure is 30 torr. C_2 is the storage capacitance per segment. Since the total storage capacitance of the charging circuit is $(C_1/2) = 3400$ pF, C_2 is 3400 pF/4 = 850 pF. At the ratio of $C_0/C_2 = 0.7$, maximum laser peak power is obtained. When small capacitance of the peaking capacitor C_0 is used for the rectangular cross-section laser, electric charge accumulated in the capacitor C_0 decreases rapidly. On the other hand, the decrease in the laser peak power at the high ratio of C_0/C_2 is due to the decrease in the breakdown voltage.

Fig. 4.4 shows the dependence of the laser peak power on the gas pressure for four types of lasers with different peaking capacitors. The charging voltage is 20 kV. When the capacitance of the peaking capacitor is increased, the optimum pressure for the laser peak power changes to lower pressure. This is because when the peaking capacitance C_0 is increased, the breakdown voltage decreases.
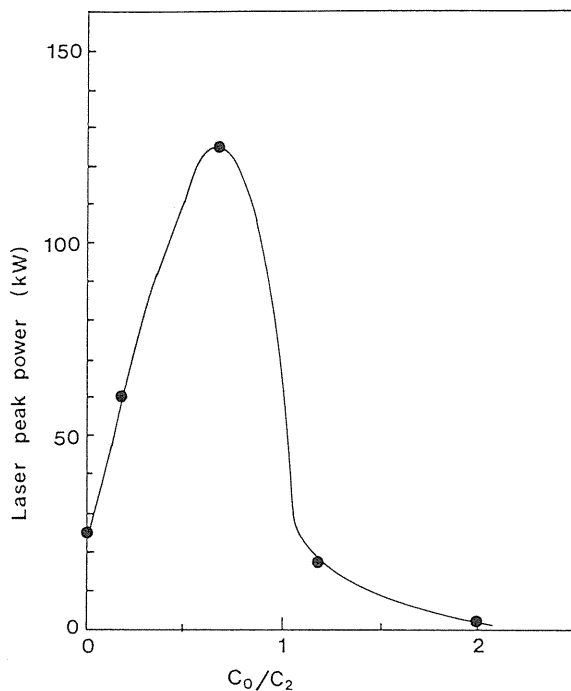
Fig. 4.3. Dependence of the laser peak power on the peaking capacitor. Charging voltage 20 kV. Gas pressure 30 torr. C_2 is the storage capacitor per segment. $C_2 = (C_1/2)/4 = 850\,\text{pF}$.
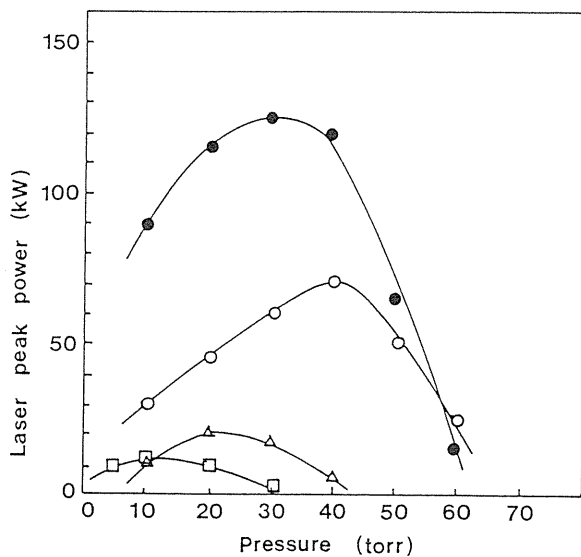

Fig. 4.4. Dependence of the laser peak power on the gas pressure for four types of lasers with different peaking capacitors. Charging voltage 20 kV. 150 pF ($\bigcirc$), 560 pF ($\bullet$), 1000 pF ($\triangle$), 1700 pF ($\square$).

Fig. 4.5 shows the dependence of the laser peak power on the wall gap (H). The charging voltage is 20 kV and the gas pressure is 30 torr. The discharge tube width (W) is 20 mm. The pulse width (FWHM) was 8 ns for each type. For the four types of laser tubes with 1, 2, 3 and 4 mm wall gaps, the laser peak powers are about 75, 125, 85 and 55 kW, respectively, and the laser peak powers per unit volume are 0.12, 0.10, 0.044 and 0.023 mJ $\cdot$ cm^{-3}, respectively. When the wall gap (H) is increased, the working volume increases. However, the laser output power per unit volume decreases. Therefore, there is an optimum wall gap for the laser peak power. In this experiment, the highest laser peak power is obtained with the laser tube of 2 mm wall gap.
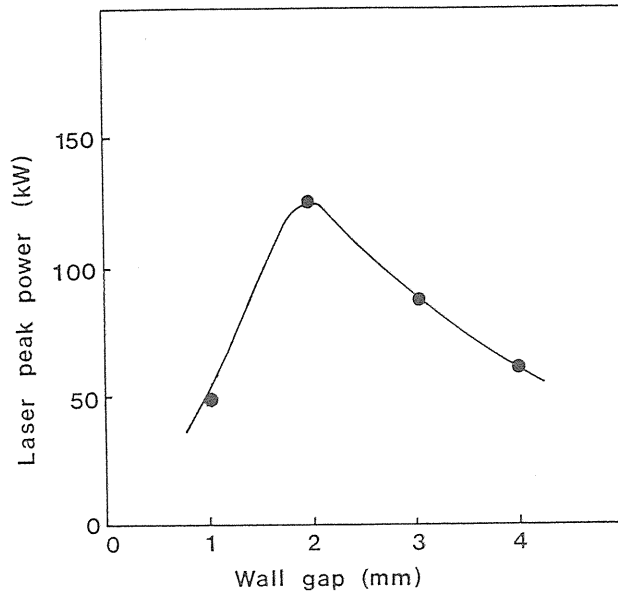

Fig. 4.5. Dependence of the laser peak power on the wall gap (H). Charging voltage 20 kV, gas pressure 30 torr, discharge tube width (W): 20 mm.

Fig. 4.6 shows the dependence of the laser peak power on the tube width (W). The charging voltage is 20 kV and the gas pressure is 30 torr. The wall gap (H) is 2 mm. The pulse width (FWHM) was 8 ns for each type. The laser output power increases with the discharge tube width. For the three types of laser tubes of $W = 10$, 20 and 30 mm, the laser peak powers are about 55, 125 and 160 kW, respectively. The highest laser output power is obtained with the laser tube of $W = 30$ mm. The laser output energy is 1.28 mJ. Higher laser output power is expected for a laser tube of larger W.

4.2.2. Comparison of the Laser Output Performance of the Low Pressure N_2 Lasers with Rectangular Cross-Section and Circular Cross-Section

Fig. 4.7 shows the time behavior of the laser pulses for the circular cross-section laser and the rectangular cross-section laser. The charging voltage is 20 kV. The gas pressure is 60 torr for the circular cross-section laser and 30 torr for the rectangular cross-section laser.
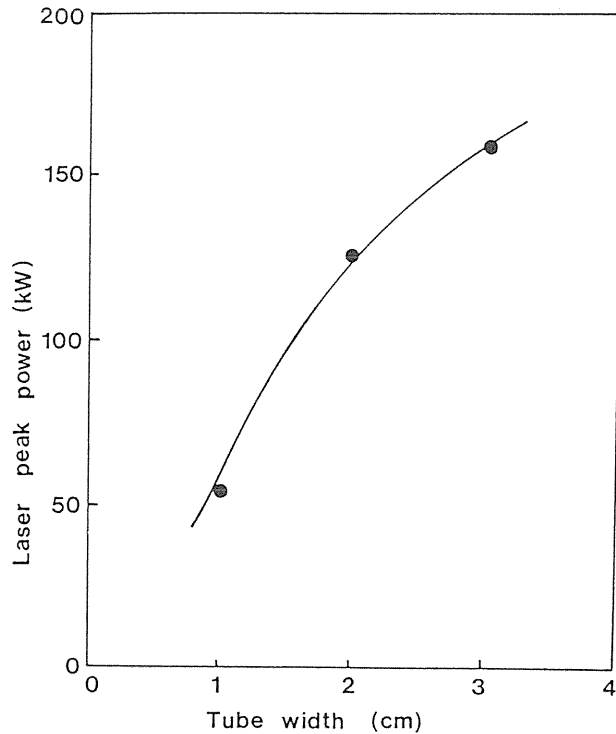
Fig. 4.6. Dependence of the laser peak power on the tube width (W). Charging voltage 20 kV, gas pressure 30 torr, wall gap (H): 2 mm.

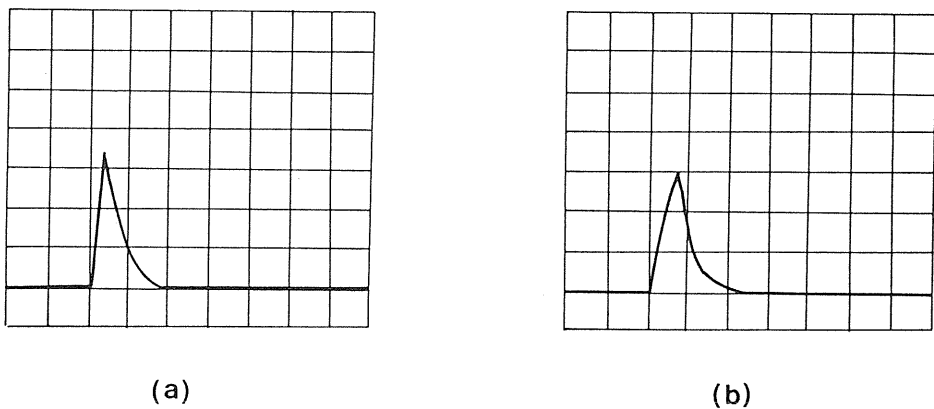**(a)**   **(b)**

Fig. 4.7. Time Behavior of the laser pulse (337 nm). Charging voltage 20 kV. (a) Circular cross-section laser (P = 60 torr), (b) rectangular cross-section laser (P = 30 torr). Horizontal axis: 10 ns/div. Vertical axis: arbitrary units.

These pressures are optimum values for laser peak power of each laser. The pulse width of the former laser is about 5 ns (FWHM), while that of the latter laser is about 8 ns (FWHM). The longer laser operation for the rectangular cross-section laser is probably due to the slow rise in electron density and the less skin depth effect. In the case of the rectangular cross-section laser of large discharge volume, the ionization is weak owing to the low discharge imped-ance. The main factor determining the laser output pulse width is the collisional mixing of the laser level by electron impact, which becomes dominant at electron density $N_e > 6 \times 10^{14}$ cm^{-3} and terminates the laser pulse. Furthermore, in the case of the circular cross-section laser, large skin depth effect occurs after the start of discharge owing to the fast increase of the discharge current. However, in the case of the rectangular cross-section laser, such skin depth effect is small, thus the laser pulse lasts for a long time.

Fig. 4.8 shows the dependence of the laser peak power on the gas pressure for the rec-tangular cross-section laser and the circular cross-section laser. The charging voltage is 20 kV. The laser peak power of the rectangular cross-section laser is higher than that of the circular cross-section laser. Furthermore, the optimum gas pressure for the laser peak power of the rectangular cross-section laser is lower than that of the circular cross-section laser. This is probably due to the low discharge impedance of the rectangular cross-section laser owing to the large discharge cross-section.
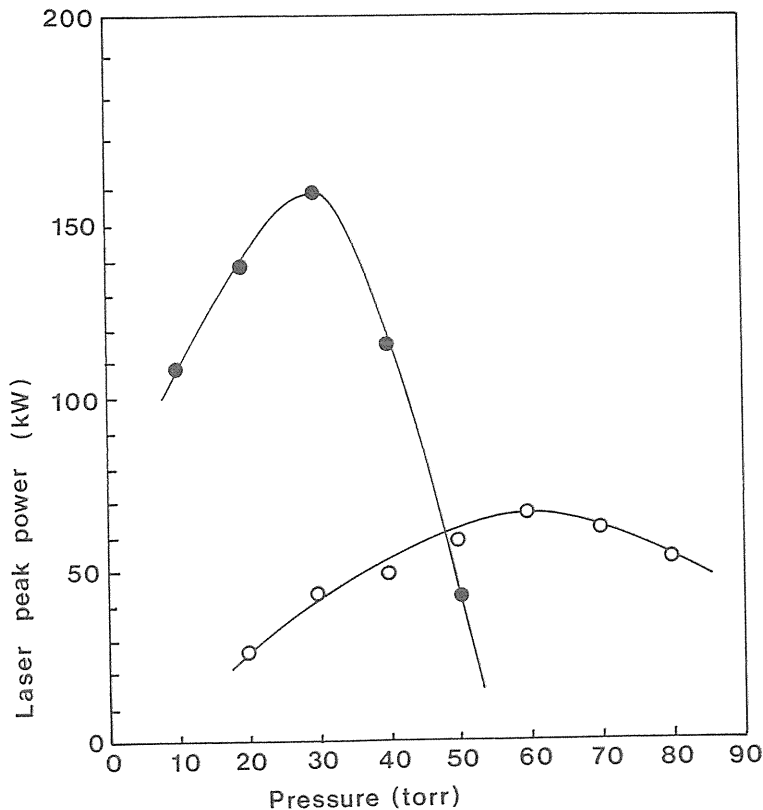

Fig. 4.8. Dependence of the laser peak power on the gas pressure for the rectangular cross-section laser (●: cross-section 2 mm × 30 mm) and circular cross-section laser (○: inner diameter 4 mm). Charging voltage 20 kV.

Table 4.1 shows the comparisons of the characteristics between the circular cross-section laser and the rectangular cross-section laser of the optimum discharge tube size and at the optimum N_2 gas pressure. The charging voltage is 20 kV. The peak output power of the rectangular cross-section laser is higher by a factor of 2.5 than that of the circular cross-section laser. Furthermore, the pulse width of the former laser is longer by a factor of 1.6 than that of the latter. As a result, the output energy of the former is larger by a factor of 4 than that of the latter. This fact also indicates that the decrease in the output power of the circular cross-section laser with large inner diameter is not only due to the decrease in the discharge impedance but also due to the concentration of the discharge near the tube wall.

Table 4.1. Characteristics of the circular cross-section laser and rectangular cross-section laser.

	Circular (4 mm I.D.)	Rectangular (2 mm × 30 mm)
discharge volume	$3.3\,cm^3$	$15.6\,cm^3$
pressure	60 torr	30 torr
pulse width (FWHM)	5 ns	8 ns
peak output power	65 kW	160 kW
peak output power per unit volume	$20\,kW \cdot cm^{-3}$	$10\,kW \cdot cm^{-3}$
output energy	0.33 mJ	1.28 mJ
output energy per unit volume	$0.1\,mJ \cdot cm^{-3}$	$0.08\,mJ \cdot cm^{-3}$

4.3. Conclusion

The output energy of 1.28 mJ was obtained by using the longitudinal discharge N_2 laser with rectangular cross-section. The laser output energy was larger by a factor 4 than that of the circular cross-section laser. The reported output energies of longitudinal discharge N_2 lasers with the active length below 30 cm are below 1 mJ,[23)-25)] thus the laser performance of this rectangular cross-section laser system is excellent. Higher laser output power is expected for a laser tube of larger width.

5. High Repetition-Rate Operation of the Longitudinal Discharge UV Laser

In some applications of UV lasers, operation at high repetition rate is desired. For example, high repetition-rate operation enables rapid data collection and fast direct-write surface processing. Longitudinal discharge laser system is favorable for high repetition rate operation, because deactivation on the tube wall is rapid and the heat transfer of the gas from the tube wall is fast.[47)-53)] However, the operation at high repetition rate of the longitudinal discharge UV lasers was not investigated in detail yet.

Normally, the repetition rate of the triggered spark gap switch is limited to 100 pps. To operate a laser at the repetition rate above 100 pps, a thyratron switch which can run at the repetition rate up to 10 kpps is used. In this chapter, the characteristics of the laser performance of the N_2 and XeCl excimer lasers at the high repetition rate using a thyratron switch are investigated.

5.1. Experimental

Fig. 5.1 shows a schematic diagram of the excitation circuit and laser tube structure of the rectangular cross-section N_2 laser using a thyratron switch. The tube structure is the same

as that of the rectangular cross-section laser tube described in chapter 4. The wall gap (H) is 2 mm and the tube width (W) is 30 mm. One segment of the tube has a length of 65 mm. The capacitances of the peaking capacitor C_0 and storage capacitor C_1 are 560 pF and 3400 pF, respectively. The thyratron is a ceramic-metal deuterium-filled thyratron LS-4111 (EG&G). In chapter 4, high voltage of 1.6×20 kV (maximum) has been supplied from LC inversion pulse generator. However, in these experiments the storage capacitor is charged directly to 40 kV (maximum). A gas flow system of about $1 1 \cdot s^{-1}$ (maximum) is used.
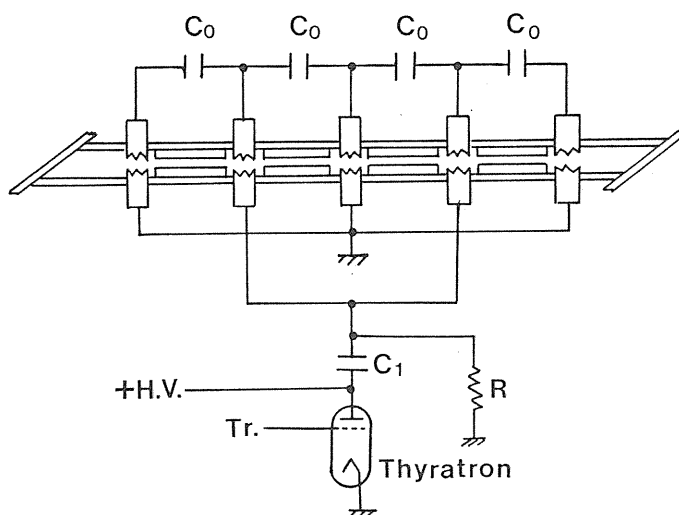

Fig. 5.1. Schematic diagram of the excitation circuit and laser tube structure. $C_0 = 560$ pF, $C_1 = 3400$ pF.

In the case of the longitudinal discharge XeCl excimer laser, the circular cross-section laser tube described in chapter 2 is used. The inner diameter of the discharge tube is 4 mm and one segment of the tube has a length of 65 mm. The gas mixture of Xe, HCl and He is stored in a tank of 3.8 liter and circulated by a diaphragm pump at about $300\ cm^3 \cdot s^{-1}$ (maximum). The optical resonator is composed of two external dielectric mirrors, one of which is a total reflector and the other is a 95% partial reflector. The excitation circuit and the electric circuit parameters are the same as that of the N_2 laser system using a thyratron switch.

5.2. Results and Discussion

5.2.1. Longitudinal Discharge N_2 Laser

The characteristics of the laser peak power obtained using a direct high-voltage pulse generator with the thyratron switch are compared with those using an LC inversion pulse generator. Fig. 5.2 shows the dependence of the laser peak power on the N_2 gas pressure for the two types of pulse generators at the same stored energy. For the direct high-voltage pulse generator, the capacitance of the storage capacitor is 3.4 nF, and the charging voltage is 40 kV, therefore the stored energy is $1/2 \times 3.4$ nF $\times (40$ kV$)^2 = 2.72$ J. For the LC inversion pulse generator, the capacitance of the storage capacitor is 13.6 nF, and the charging voltage

is 20 kV, therefore the stored energy is also $1/2 \times 13.6\,\text{nF} \times (20\,\text{kV})^2 = 2.72\,\text{J}$. The maximum laser peak powers with the direct high-voltage pulse generator and with LC inversion pulse generator are about 170 kW and 160 kW, respectively, and the pulse widths both were about 8 ns. The laser energies with these pulse generators were 1.36 mJ and 1.28 mJ, respectively. The higher laser energy with the direct high-voltage pulse generator is due to the higher driving voltage of the pulse generator. As discussed in chapter 3, in the case of the LC inversion pulse generator, when the storage capacitor is charged at 20 kV, the driving voltage is about 32 kV. However, in the case of the direct high-voltage pulse generator, when the storage capacitor is charged at 40 kV, the driving voltage is about 40 kV.
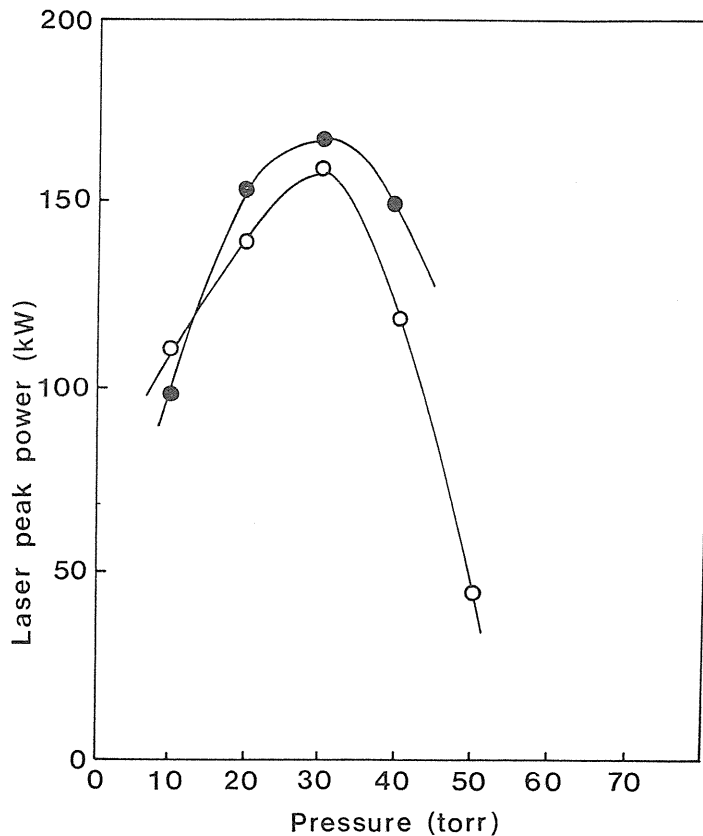

Fig. 5.2. Dependence of the laser peak power on the gas pressure for the two types of excitation circuits using the LC inversion pulse generator with spark gap switch (○) and using the direct high-voltage pulse generator with a thyratron (●) at the same stored energy. Stored energy: $1/2 \times 13.6\,\text{nF} \times (20\,\text{kV})^2 = 1/2 \times 3.4\,\text{nF} \times (40\,\text{kV})^2 = 2.72\,\text{J}$. Repetition rate 10 pps.

Fig. 5.3 shows the dependence of the laser peak power on the N_2 gas pressure for the two types of the pulse generators at the driving voltage of 32 kV. The stored energies in the direct high-voltage pulse generator and LC inversion pulse generator are $1/2 \times 3.4\,\text{nF} \times (32\,\text{kV})^2 = 1.74\,\text{J}$ and $1/2 \times 13.6\,\text{nF} \times (20\,\text{kV})^2 = 2.72\,\text{J}$, respectively. The laser output

energy with the direct high-voltage pulse generator is lower than that with the LC inversion pulse generator. This is because the inductance of the direct high-voltage pulse generator is larger than that of the LC inversion pulse generator. However, the efficiency of the laser system using the direct high-voltage pulse generator is higher than that using the LC inversion pulse generator, because the stored energy in the direct high-voltage pulse generator is 36% lower than that in the LC inversion pulse generator at the same driving voltage.
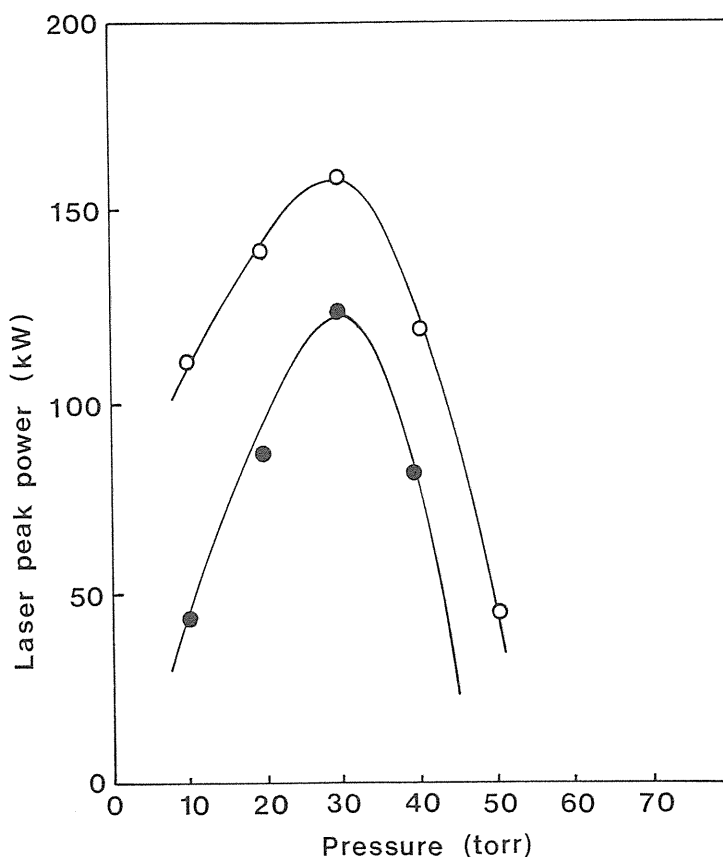

Fig. 5.3. Dependence of the laser peak power on the gas pressure for the two types of excitation circuits using the LC inversion pulse generator with spark gap switch (○) and using the direct high-voltage pulse generator with a thyratron (●) at the same driving voltage of 32 kV. Repetition rate 10 pps.

Fig. 5.4 shows the dependence of the laser peak power of the direct pulse generator on the charging voltage at the gas pressure of 30 torr. The laser peak power increases as the voltage increases.

The dependences of the laser peak power and the average laser power on the repetition rate are shown in Figs. 5.5 and 5.6, respectively. (○: charging voltage of 40 kV, the gas flow rate of $1 \, l \cdot s^{-1}$, ●: charging voltage of 32 kV, the gas flow rate of $1 \, l \cdot s^{-1}$, □: charging voltage
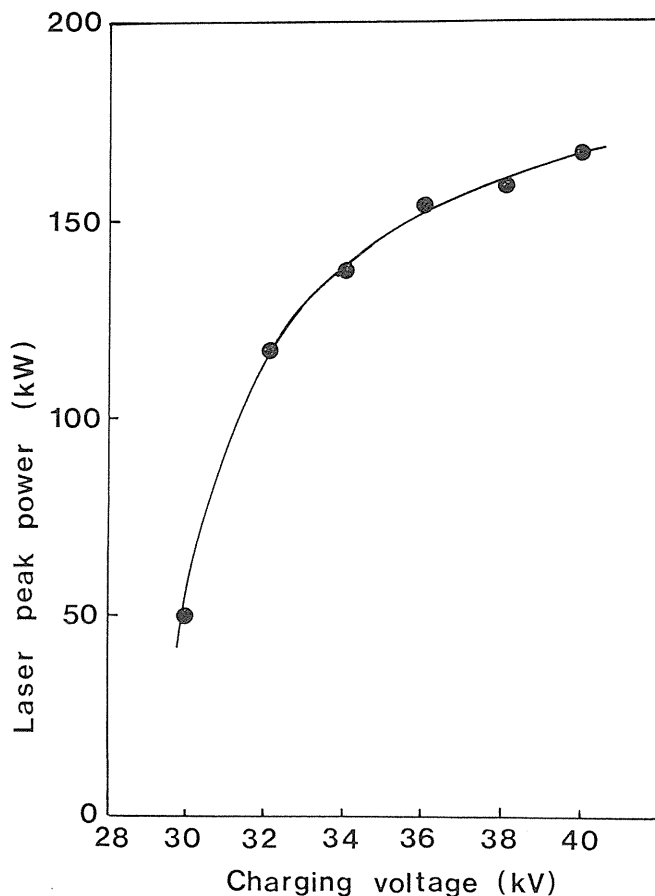
Fig. 5.4. Dependence of the laser peak power on the charging voltage at the gas pressure of 30 torr.

of 40 kV, no gas flow system) The gas pressure is 30 torr. By using the gas flow system, high repetition rate operation is realized. When the laser system is operated at the charging voltage of 40 kV with the gas flow system, maximum average power of 65 mW is obtained at the repetition rate of 80 pps. When it is operated at the charging voltage of 32 kV, maximum average power over 100 mW is obtained at the repetition rate of 130 pps.

At high repetition rate the laser peak power decreases. The reasons of that decrease are believed to be as follows.

(a) Decrease in the gain of the lasing transition[48),49)]

In detailed analysis, the gain of an electronic-vibrational-rotational transition in a N_2 molecule depends on translational temperature, vibrational temperature and the density of molecules in the ground electronic states which may vary with increasing the repetition rate of pumping pulse.

The vibrationally excited molecules can be deactivated both in the bulk (homogeneous relaxation) and on the surface of the confining walls (heterogeneous relaxation). The characteristic time for homogeneous vibrational relaxation at a N_2 gas pressure of several tens torr
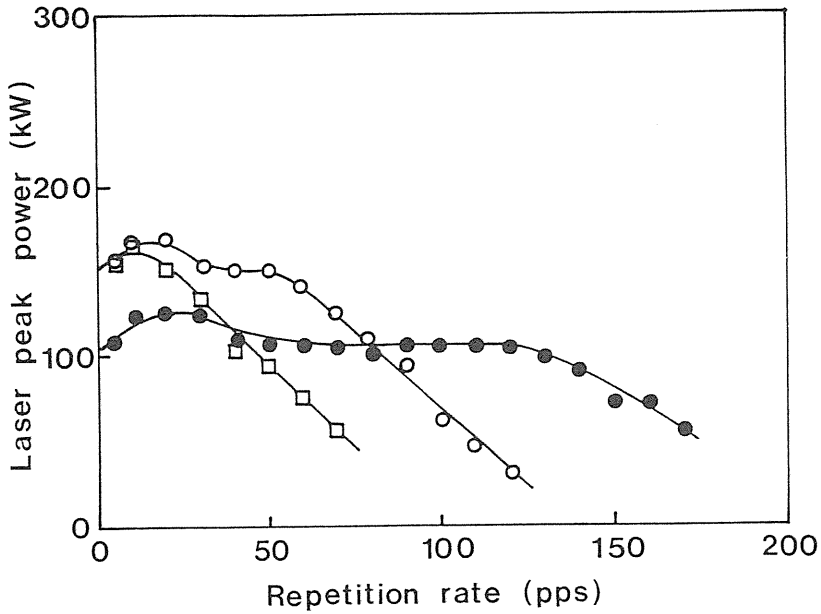
Fig. 5.5. Dependence of the laser peak power on the repetition rate at the gas pressure of 30 torr. Using a gas-flow system (○) and not using a gas-flow system (□) at the charging voltage of 40 kV. Using a gas-flow system at the charging voltage of 32 kV (●).
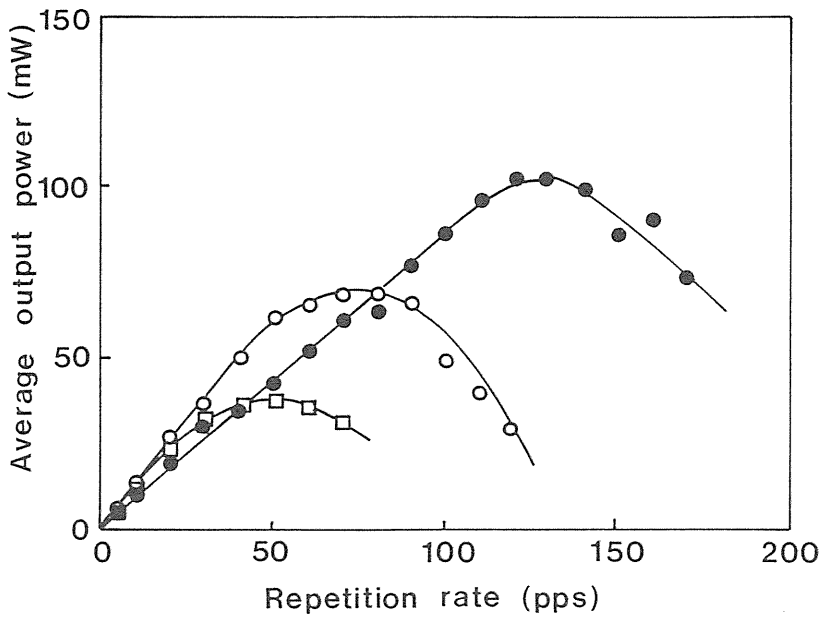

Fig. 5.6. Dependence of the average laser power on the repetition rate at the gas pressure of 30 torr. Using a gas-flow system (○) and not using a gas-flow system (□) at the charging voltage of 40 kV. Using a gas-flow system at the charging voltage of 32 kV (●).

and temperatures of 300–500° K is above 1 s.[48] However, the time required for diffusion of the molecules to the walls is by many orders of magnitude shorter than the volume relaxation time. Therefore, it may be postulated that heterogeneous deactivation of the vibrationally excited molecules should play a more important part. The characteristic heterogeneous relaxation time is calculated as below.[50]

$$\tau_p \sim r/\gamma c \qquad\qquad\qquad (5.1)$$

where r is the wall gap of the discharge tube; c is the rms molecular velocity; γ is the heterogeneous vibrational deactivation probability. In this case, using the value of γ for Pyrex ($\sim 4.5 \times 10^{-4}$), the deactivation time is estimated of several msec.[50] From this estimation, it can be concluded that the vibrational energy relaxes slowly, and the vibrational temperature will influence the gain and laser output at the pulse repetition rate of several hundreds pps.

The increase in the density of metastable excited N_2 molecules with increasing repetition rate may decrease the N_2 molecules in the ground electronic state and reduce the gain and laser output. The formation of the excited molecules is about 2–4% per pulse.[48] In detailed analysis, the role of metastable excited N_2 molecules will be negligible up to repetition rate of several tens of kpps, because the deactivation time is very short or the density is very low.[48]

The energy dissipated in translational heating of the gas as a result of elastic collisions between electrons and molecules amounts to several tenths of percent of the total input energy. However, the direct gas heating by this mechanism is small and negligible.[48] The gas heating is done by several steps. First, most of the input energy is dissipated in vibrational and electronic excitation of the molecules which relax mainly at the discharge tube walls, and the walls are heated. Second, the heat energy of walls is dissipated in translational heating of the gas inside the tube. Consequently, almost all the energy supplied to the gas is dissipated in translational heating.

(b)   Degradation of the uniformity of the discharge[51]

At high repetition rate, the residual ions and electrons will degrade the uniformity of the electric discharge. The ions and electrons relax mainly at the tube wall, and the relaxation time is several msec.[51] Therefore, they will influence the uniformity of the discharge at the repetition rate of several hundreds pps, and reduce the laser output power.

(c)   Decrease in the breakdown voltage

At high repetition rate, the residual ions and electrons will also lead to the decrease in the breakdown voltage. It causes a decrease in electron temperature. Therefore, it will influence the formation of the population inversion and reduce the laser output power.

In this experiment, the laser peak power decreases at the repetition rate above 140 pps, but the breakdown voltage is not influenced by the repetition rate. This suggests that the problems of the rise in the translational and vibrational temperatures and the degradation of the discharge uniformity are essential. When the temperature of the tube was increased, the laser output power decreased significantly. Furthermore, higher repetition rate operation is obtained by operating at 32 kV rather than at 40 kV. Thus the decrease in the gain owing to the rise in the translational temperature is one of the main factor limiting the repetition rate.

Therefore, by cooling the laser discharge tube, using smaller inner diameter tube made of materials of the high vibrational deactivation probability and thermal conductivity, and using a high speed gas flow system, operations at several kpps will be possible.

5.2.2.   Longitudinal Discharge XeCl Excimer Laser

The laser output power of the longitudinal discharge XeCl excimer laser using the direct

high voltage pulse generator was almost the same as that using the tow-stage Marx bank generator.

The dependences of the laser peak power and the average laser power on the repetition rate are shown in Figs. 5.7 and 5.8, respectively. The gas pressure is 1.3 atm (He:Xe:HCl = 1.3 atm:6.0 torr:2.4 torr) and the charging voltage is 40 kV. The laser peak power decreases as the repetition rate increases above 30 pps. As a result, the average output power has a maximum value at 80 pps. The decrease in the laser peak power at high repetition rate is due to the degradation of the uniformity of the discharge.[54] In the report by Sze et al., where a high-repetition-rate miniature discharge device was discussed, four times of discharge volume clearance by the gas flow between two successive discharges were necessary.[54] In the case of this experiment, the replacement rate of the gas is $300 \, cm^3 \cdot s^{-1}/3.3 \, cm^3 = 91 \, s^{-1}$, thus the limit of the repetition rate by the discharge clearance is about $91 \, s^{-1}/4 = 23$ pps.

On the other hand, Christensen estimated the characteristic diffusion time as[55]

$$t \sim W^2/4D \qquad (5.2)$$

where W is the characteristic channel dimension and D is the diffusion coefficient. In the case of this experiment, W and D are 1 mm and $0.63 \, cm^2 \cdot s^{-1}$ (He gas at the pressure of 1.3 atm and temperature of 300 K), respectively. Substituting these values for the equation (5.2), t is
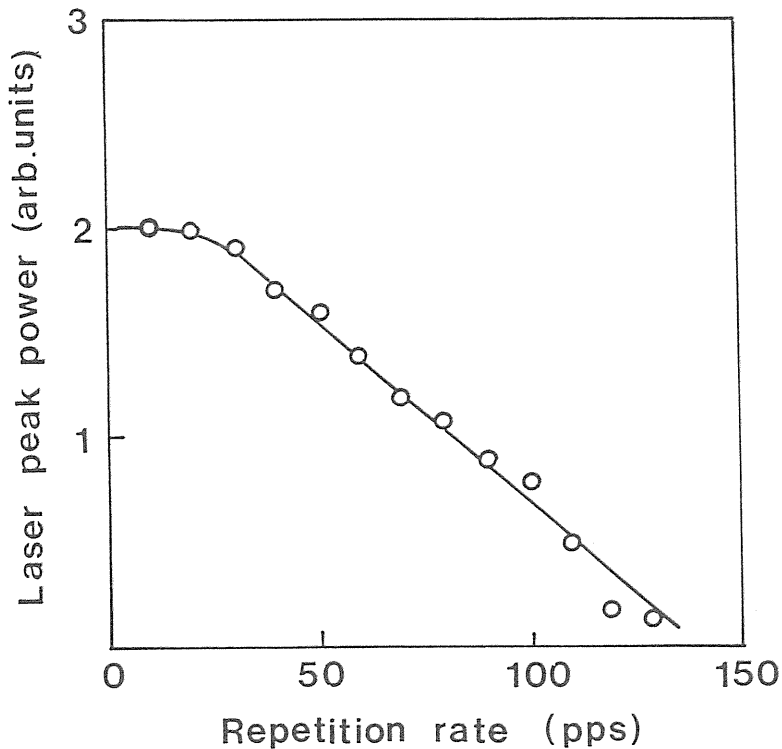

Fig. 5.7. Dependence of the laser peak power on the repetition rate at the gas pressure of 1.3 atm (He:Xe:HCl = 1.3 atm:6 torr:2.4 torr) and charging voltage of 40 kV.
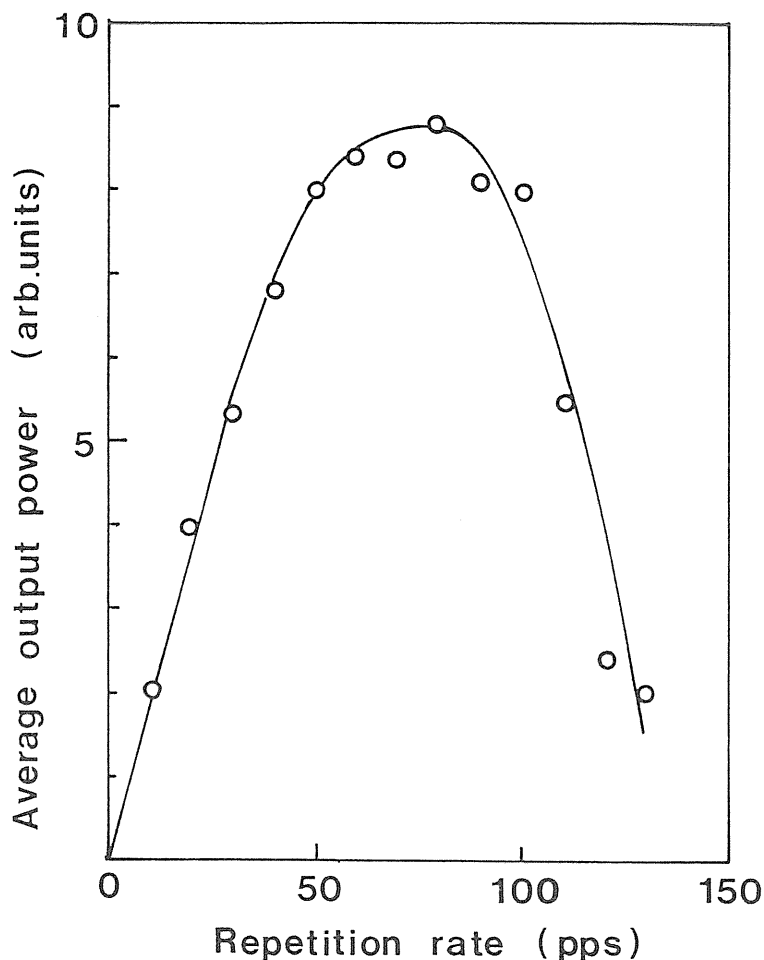
Fig. 5.8. Dependence of the average output power on the repetition rate at the gas pressure of 1.3 atm (He:Xe:HCl = 1.3 atm:6 torr:2.4 torr) and charging voltage of 40 kV.

calculated to be 4 ms. Therefore, if it is assumed that several times as long as the characteristics diffusion time is required, the repetition rate will be limited to several tens pps.

As discussed above, the repetition rates limited by the time required for the discharge volume clearance and the characteristic diffusion time are several tens pps. The laser peak power in this experiment decreases at the repetition rate of several tens pps, and it is consistent with the estimation. To achieve high repetition rate operation of kpps, it is necessary to use gas circulation system of high velocity or to use the discharge tube of small inner diameter.

5.3. Conclusion

The characteristics of the performance of the N_2 and XeCl excimer lasers using a direct high-voltage pulse generator with a thyratron switch have been investigated at high repetition

rate. The maximum average output power above 100 mW was obtained at the repetition rate of 130 pps by N_2 laser. The laser average output power of XeCl excimer laser had a maximum at the repetition rate of 80 pps. By using the gas circulation system of higher velocity or by selecting a best discharge tube material, higher repetition rate operation will be possible.

6. Summary

The design and construction of the longitudinal discharge pulsed UV laser with automatic spark UV preionization have been described, and the lasing of compact XeCl and N_2 lasers from this laser system have been reported. This is the first time that spark UV preionization was used for longitudinal discharge lasers. By using spark UV preionization and a charge transfer excitation circuit, the laser performance has been considerably improved.

First, the technique was applied to a XeCl excimer laser, and the parameters were optimized. As a result, laser pulses of about 200 μJ output energy and 15 ns width (FWHM) were obtained. The output peak power per unit length and the efficiency are better than those reported by Zhou et al.[20] which is the only one reported so far as a longitudinal discharge XeCl excimer laser.

Next, it was applied to a low pressure N_2 laser. Furthermore, the impedance of the excitation circuit has been decreased by developing an LC inversion—charge transfer excitation circuit. By using this excitation circuit and the spark UV preionization, the laser performance of the longitudinal discharge N_2 laser was considerably improved. The characteristics of the laser output power from the longitudinal discharge N_2 laser have been investigated qualitatively, and it was shown that the improvement of the laser performance with the spark UV preionization and the charge transfer circuit is mainly due to the high electron density.

An attempt to increase the output energy of the longitudinal discharge N_2 laser with circular cross-section has been carried out by increasing the inner diameter of the discharge tube which leads to an increase in working volume. However, there was an optimum inner diameter of 4 mm, and no appreciable increase of the laser energy was observed for larger inner diameter.

When the inner diameter of the discharge tube was increased, there was an optimum value. The reason of the results has been discussed in detail by using a computer simulation. It has been proved that skin depth effect is significant to the discharge and excitation of the N_2 molecules in the discharge tube. Thus, to avoid the skin depth effect, a longitudinal discharge N_2 laser with rectangular cross-section of large working volume with the short wall gap and the wide width of the discharge area has been developed, and the parameters were optimized. As a result, the output energy has been considerably improved and laser pulses of 160 kW peak power, 1.28 mJ output energy and 8 ns pulse width (FWHM) were obtained. The output energy of the rectangular cross-section laser is about 4 times larger than that of the circular cross-section laser. Although this laser performance is very excellent, higher laser output power is expected for a laser tube of larger width.

The characteristics of the laser performance of the N_2 and XeCl excimer lasers using thyratron switch at high repetition rate have been investigated. For N_2 laser, maximum average output power above 100 mW was obtained at the repetition rate of 130 pps. For XeCl excimer laser, maximum repetition rate was 80 pps.

In this work, pulsed UV lasers excited by longitudinal discharge with automatic spark UV preionization, which are simple in constructions and favorable for the compactness of UV lasers, have been constructed. For the further development, however, some future work

may be required. For the XeCl excimer laser, the maximum laser energy was about $200\,\mu$J. It is mainly limited by the relatively low discharge uniformity. Larger laser energy will be obtained with the improvement of the discharge uniformity by using stronger preionization. For the N_2 laser the maximum laser output power of 170 kW and maximum laser energy of 1.36 mJ were obtained. Although these values are very excellent for longitudinal discharge N_2 lasers of the small size, larger energy will be obtained by increasing the discharge width of the rectangular cross-section laser tube with the wall gap of 2 mm. The present laser system is compact enough for some applications. For the further compactness, the developments of the miniaturizations of power supply, capacitors and switches with good durability are desired.

The compact UV laser systems described here can be easily applied in the laboratory research. One of its most likely applications is the spectroscopy tool. Also these UV lasers are suitable for the pumping source of dye lasers, because most dyes have an absorption band at UV region. One of other applications is the first oscillator in a high power amplifier chain. The laser system described here is more compact and simpler in constructions than the other UV laser systems. Therefore, it will expand the application fields of UV laser.

Acknowledgments

References

1) Gray K. Klauminzer, Laser Focus, December, **54** (1984).
2) H.G. Heard, Nature **200**, 667 (1963).
3) Donald A. Leonald, Appl. Phys. Lett. **7**, 4 (1965).
4) R.W. Dreyfus and R.T. Hodgson, Appl. Phys. Lett. **20**, 195 (1972).
5) N.G. Basov, V.A. Danilychev, Y.M. Popov and D.D. Khodkevich, Sov. Phys. JETP Lett. **22**, 329 (1970).
6) S.K. Searles and G.A. Hart, Appl. Phys. Lett. **27**, 243 (1975).
7) J.J. Ewing and C.A. Brau, Appl. Phys. Lett. **27**, 350 (1975).
8) J.A. Mangano and J.H. Jacob, Appl. Phys. Lett. **27**, 495 (1975).
9) J.I. Levatter, J.H. Morris and Shao-Chi Lin, Appl. Phys. Lett. **32**, 630 (1978).
10) A.J. Andrews, A.J. Kearsley and C.E. Webb, Opt. Commun. **20**, 265 (1977).
11) V.N. Ishchenko, V.N. Lisitsyn and A.M. Razhev, Opt. Commun. **21**, 30 (1977).
12) R. Burnham, N.W. Harris and N. Djeu, Appl. Phys. Lett. **28**, 86 (1976).
13) Ronald W. Waynant, Appl. Phys. Lett. **30**, 234 (1977).
14) R. Burnham and N. Djeu, Appl. Phys. Lett. **29**, 707 (1976).
15) R. Burnham, Opt. Commun. **24**, 161 (1978).
16) D.G. Sutton, S.N. Suchard, O.L. Gibb and C.P. Wang, Appl. Phys. Lett. **28**, 522 (1976).
17) I.M. Isakov, A.G. Leonov and V.E. Ogluzdin, Sov. Tech, Phys. Lett. **3**, 397 (1977).
18) P. Burkhard, T. Gerber and W. Lüthy, Appl. Phys. Lett. **39**, 19 (1981).
19) D. Cleschinsky, D. Dammasch, H.J. Eichler and J. Hamisch, Opt. Commun. **39**, 79 (1981).
20) Zhenzhou Zhou, Yongjian Zeng and Mingxin Qiu, Appl. Phys. Lett. **43**, 347 (1983).
21) H.J. Eichler, J. Hamisch, B. Nagel and W. Schmid, Appl. Phys. Lett. **46**, 911 (1985).
22) H. Furuhashi, M. Hiramatsu and T. Goto, Appl. Phys. Lett. **50**, 883 (1987).

23) N.R. Nilsson, O. Steinvall, C.K. Subramanian and L. Hogberg, Physica Scripta 1, 153 (1970).
24) C. Lai and S.N. Thakur, Indian J. Phys. 59B, 129 (1985).
25) L.R. Lidholt, Rev. Sci. Instrum. 43, 1765 (1972).
26) T.S. Fahlen, IEEE J. Quantum Electron. QE-15, 311 (1979).
27) S.C. Lin and J.I. Levatter, Appl. Phys. Lett. 34, 505 (1979).
28) V.E. Peet and A.B. Treshchalov, Sov. J. Quantum Electron. 15, 1613 (1985).
29) A.B. Treshchalov, V.E. Peet and V.T. Mihkelsoo, IEEE J. Quantum Electron. QE-12, 51 (1986).
30) H. Hokazono, K. Midorikawa, M. Obara and T. Fujioka, J. Appl. Phys. 56, 680 (1984).
31) P. Burlamacchi and R. Salimbeni, Opt. Commun. 26, 233 (1978).
32) R.C. Sze and P.B. Scott, Appl. Phys. Lett. 33, 419 (1978).
33) M. Ohwa and M. Obara, J. Appl. Phys. 59, 21 (1986).
34) R.C. Sze, J. Appl. Phys. 50, 4596 (1979).
35) M.R. Osborne and M.H. Hutchinson, J. Appl. Phys. 59, 711 (1986).
36) M.R. Osborne, J. Coutts, M.H.R. Hutchinson and C.W. Webb, Appl. Phys. Lett. 49, 7 (1986).
37) M. Hiramatsu, H. Furuhashi and T. Goto, J. Appl. Phys. 59, 1946 (1986).
38) R. Tennant, Laser Focus, October, 65 (1981).
39) W.A. Fitzsimmons, L.W. Anderson, C.E. Riedhauser and J.M. Vertilek, IEEE J. Quantum Electron. QE-12, 624 (1976).
40) D.C. Cartwright, J.Appl. Phys. 49, 3855 (1978).
41) W. Benesch, J.T. Vanderslice, S.G. Tilford and P.G. Wilkinson, Astrophys. J. 143, 236 (1966).
42) K.H. Wagner, Z. Physik. 178, 64 (1964).
43) P. Felsenthal and J. Proud, Phys. Rev. 139, A1796 (1965).
44) A.W. Ali, A.C. Kolb and A.D. Andersson, Appl. Opt. 6, 2115 (1967).
45) R.S. Kunabenchi, M.R. Gorbal and M.I. Savadatti, Prog. Quant. Electr. 9, 259 (1984).
46) D.A. Leonard, Appl. Phys. Lett. 7, 4 (1965).
47) M. Feldman, P. Lebow, F. Raab and H. Metcalf, Appl. Opt. 17, 774 (1978).
48) A.N. Sviridov and Yu. D. Troikhin, Sov. J. Quantum Electron. 8, 1136 (1978).
49) A.N. Sviridov and Yu. D. Troikhin, Sov. J. Quantum Electron. 8, 1177 (1978).
50) J.E. Morgan and H.I. Schiff, Can. J. Chem. 41, 903 (1963).
51) R. Targ, IEEE J. Quantum Electron. QE-8, 726 (1972).
52) V.G. Il'yushko and V.F. Kravchenko, Sov. J. Quantum Electron. 17, 1407 (1987).
53) Yu.I. Bychkov, M.N. Kostin, V.F. Losev and V.F. Tarasenko, Institute of Atmospheric Optics, 1093 (1979).
54) R.C. Sze and E. Seegmiller, IEEE J. Quantum Electron. QE-17, 81 (1981).
55) C.P. Christensen, Appl. Phys. Lett. 30, 483 (1977).